Geochemistry, Geophysics, Geosystems®

AGU ADVANCING EARTH AND SPACE SCIENCE

RESEARCH ARTICLE
10.1029/2021GC010158

Special Section:
Cenozoic Evolution of Mountains, Monsoons, and the Biosphere

Zircon U-Pb Age Constraints on NW Himalayan Exhumation From the Laxmi Basin, Arabian Sea

Peng Zhou[1,2], Daniel F. Stockli[3], Thomas Ireland[4], Richard W. Murray[5], and Peter D. Clift[1]

[1]Department of Geology and Geophysics, Louisiana State University, Baton Rouge, LA, USA, [2]Department of Physics, Geology, and Engineering Technology, Northern Kentucky University, Highland Heights, KY, USA, [3]Department of Geological Sciences, Jackson School of Geosciences, University of Texas at Austin, Austin, TX, USA, [4]Department of Earth and Environment, Boston University, Boston, MA, USA, [5]Woods Hole Oceanographic Institution, Woods Hole, MA, USA

Abstract The Indus Fan, located in the Arabian Sea, contains the bulk of the sediment eroded from the Western Himalaya and Karakoram. Scientific drilling in the Laxmi Basin by the International Ocean Discovery Program recovered a discontinuous erosional record for the Indus River drainage dating back to at least 9.8 Ma, and with a single sample from 15.6 Ma. We dated detrital zircon grains by U-Pb geochronology to reconstruct how erosion patterns changed through time. Long-term increases in detrital zircon U-Pb components of 750–1,200 and 1,500–2,300 Ma record increasing preferential erosion of the Himalaya relative to the Karakoram between 8.3–7.0 and 5.9–5.7 Ma. The average contribution of Karakoram-derived sediment to the Indus Fan fell from 70% of the total at 8.3–7.0 Ma to 35% between 5.9 and 5.7 Ma. An increase in the contribution of 1,500–2,300 Ma zircons starting between 2.5 and 1.6 Ma indicates significant unroofing of the Inner Lesser Himalaya (ILH) by that time. The trend in zircon age spectra is consistent with bulk sediment Nd isotope data. The initial change in spatial erosion patterns at 7.0–5.9 Ma occurred during a time of drying climate in the foreland. The increase in ILH erosion postdated the onset of dry-wet glacial-interglacial cycles suggesting some role for climate control. However, erosion driven by rising topography in response to formation of the ILH thrust duplex, especially during the Pliocene, also played an important role, while the influence of the Nanga Parbat Massif to the total sediment flux was modest.

Plain Language Summary Mountain belts are constructed by tectonic forces from within the solid Earth modulated by surface processes. The Himalaya represents the type example of such interactions, where the growth of the mountains and the Asian monsoon interact. Sediments from the Arabian Sea allow the long-term erosion patterns of the NW Himalaya to be reconstructed. We use the crystallization age of zircon sand grains in sediment dating back to 15.6 Ma to see how the erosion has changed in response to the evolving climate. There is a trend toward more erosion from the Himalaya and less from the Karakoram starting around 8.3–7.0 Ma, which was a time of transition toward a drier climate in the NW Himalaya. Furthermore, we see a sharp increase in erosion from the Inner Lesser Himalaya starting between 2.5 and 1.6 Ma. This was caused by the formation of a thrust duplex pushing up these ranges, which in turn focused orographic precipitation. The timing of this exposure is much younger than understood from studies of sedimentary rocks in the foreland basin onshore. Our study highlights the role that tectonics plays in controlling what parts of the mountain belt are subject to the fastest erosion.

Key Points:

- Geochronologic analyses show increased relative erosion from the Himalaya compared to the Karakoram between 8.3–7.0 Ma and 5.9–5.7 Ma
- Changing patterns of erosion correlate with climatic drying at ~7.7–5.9 Ma and relate to solid Earth tectonic forces building topography
- Erosion from the Inner Lesser Himalaya increased between 2.5 and 1.6 Ma on a regional scale

Supporting Information:

Supporting Information may be found in the online version of this article.

Correspondence to:

P. D. Clift,
pclift@lsu.edu

Citation:

Zhou, P., Stockli, D. F., Ireland, T., Murray, R. W., & Clift, P. D. (2022). Zircon U-Pb age constraints on NW Himalayan exhumation from the Laxmi Basin, Arabian Sea. *Geochemistry, Geophysics, Geosystems*, *23*, e2021GC010158. https://doi.org/10.1029/2021GC010158

Received 9 SEP 2021
Accepted 10 DEC 2021

Author Contributions:

Conceptualization: Peter D. Clift
Formal analysis: Daniel F. Stockli, Thomas Ireland, Richard W. Murray, Peter D. Clift
Funding acquisition: Peter D. Clift
Supervision: Peter D. Clift

1. Introduction

Collision between India and Eurasia, starting about 50–60 Ma (Garzanti et al., 1987; Jaeger et al., 1989; Najman et al., 2010), has resulted in formation of the largest mountain ranges on Earth. The Himalaya have continued to evolve both in topography and structure as a result of ongoing tectonic deformation coupled with erosion, which is partly modulated by the strength of summer monsoon rains (Bookhagen et al., 2005; Clift, Hodges, et al., 2008; Wobus et al., 2003). Sediments eroded from the Western Himalaya has been deposited in the Arabian Sea where they form the second largest sediment body on Earth, the Indus submarine fan (Clift et al., 2001; Kolla & Coumes, 1987). Despite extensive studies on the foreland basin, a regional erosion history for the Western Himalaya has not yet been generated, hampering efforts to understand what controls orogenic evolution on multi-million year timescales.

Writing – original draft: Daniel F. Stockli, Thomas Ireland, Richard W. Murray, Peter D. Clift
Writing – review & editing: Daniel F. Stockli, Richard W. Murray, Peter D. Clift

The sedimentary deposits of the Indus Fan represent an archive of the erosion and weathering processes in the Western Himalaya since the onset of continental collision, at least since ~45 Ma (Clift et al., 2001). While bedrocks exposed at the surface in the mountains can be used to reconstruct the uplift and exhumation of those particular rock formations, the submarine fan sedimentary record captures spatial and temporal variations spanning the long-term history of denudation, albeit one buffered by sediment transport processes. Because some of the bedrock sources have been completely removed by erosion, so that their exhumation history no longer accessible, the sedimentary record becomes the only archive of the earlier erosion and exhumation history. Although this record is partially available in the Himalayan foreland basin, these proximal, continental, syn-tectonic deposits are more difficult to date at high resolution, and the sequences are truncated by unconformities and deformed by progressive incorporation into the sub-Himalayan fold and thrust belt (Najman, 2006). Moreover, any given section in the accreted foreland basin can only represent the sediment derived from paleo-rivers that once flowed in front of the mountains in that region. As such, any given section must preserve a history of erosion in a limited catchment draining a particular part of the mountains and not provide a more integrated orogen-scale overview.

Sediment from the Western Himalaya is delivered to the Arabian Sea by the Indus River and its eastern tributaries in the Punjab (Figure 1a). The Indus is particularly sensitive to variations in the strength of the Asian monsoon because it is situated on the western edge of the region affected by this climatic phenomenon. As a result, variations in monsoon strength can have a major impact on both patterns and rates of erosion in the various ranges that comprise the western end of the Himalayan mountain chain (Figure 1b). A number of studies have suggested that changes in monsoon intensity have significantly impacted the erosion history of the Western Himalaya (Bookhagen et al., 2005; Clift, Giosan, et al., 2008; Clift, Hodges, et al., 2008).

Debate continues regarding what controls Himalayan erosion, with some workers favoring tectonic processes that drive rock uplift (Burbank et al., 2003), as being the critical control, while others have argued for a dominance by monsoon rainfall and/or glaciation (Whipple, 2009; Wobus et al., 2003). These focus erosion and restrict sediment producing regions into a relatively narrow band of the range front and in turn promote exhumation of deep buried rocks (Thiede et al., 2004). It is however known that the erosion in the Himalaya is sensitive to climate change because sediment supply during and shortly after the Last Glacial Maximum (LGM) appears to have been preferentially focused in the Karakoram, while the strongest erosion shifted into the Lesser Himalaya after the onset of the Holocene (Clift, Giosan, et al., 2008).

In this study, we focus on the Late Miocene-Recent history and examine evidence for coupling between the tectonic evolution and the changing strength of summer monsoon rains. We take advantage of recently a recovered sedimentary record collected by the International Ocean Discovery Program (IODP) in 2015 from the Eastern Arabian Sea, which provides an archive of erosion extending back to at least ~9.8 Ma, with one sample dated at ~15.6 Ma (Pandey et al., 2016d). An earlier lower-resolution study using limited detrital zircon grains and more numerous bulk sediment Nd and Sr isotopes argued that changes in erosion across the Indus Basin were not connected to climate change and largely reflected increasing erosion of the Lesser Himalaya, especially starting at 1.9 Ma (Clift et al., 2019). We test this model using an expanded set of new U-Pb ages from detrital zircon sand grains (1,882 new ages from 15 additional samples, supplementing 1,335 ages from 10 samples in the earlier work) coupled with a more sophisticated statistical treatment of the total data set to reconstruct the evolving patterns of erosion.

2. Geologic Setting

The sediments analyzed in this study were retrieved from the Laxmi Basin in the Eastern Arabian Sea (Figures 1a and 1b). This basin is separated from the rest of the Arabian Sea by a continental block known as Laxmi Ridge (Pandey et al., 1995). Rifting in Laxmi Basin preceded the breakup of the main Arabian Basin, west of Laxmi Ridge, and likely occurred in the latest Cretaceous (Bhattacharya et al., 1994; Radhakrishna et al., 2021). Since that time 2–3 km of sediment have accumulated in the Laxmi Basin. Initial provenance investigation of these sediments using Nd isotopes and limited zircon U-Pb dating indicated that while some fine-grained material might be derived from peninsular India most of the sediment was sourced from the Indus Delta, located around 800 km toward the north (Clift et al., 2019). Continuous sedimentation in Laxmi Basin was interrupted by the emplacement of a large mass transport complex (MTC) likely just before 10.8 Ma and definitely before 9.8 Ma, which eroded most of the Middle Miocene at Site U1456 (Calvès et al., 2015; Dailey et al., 2019).

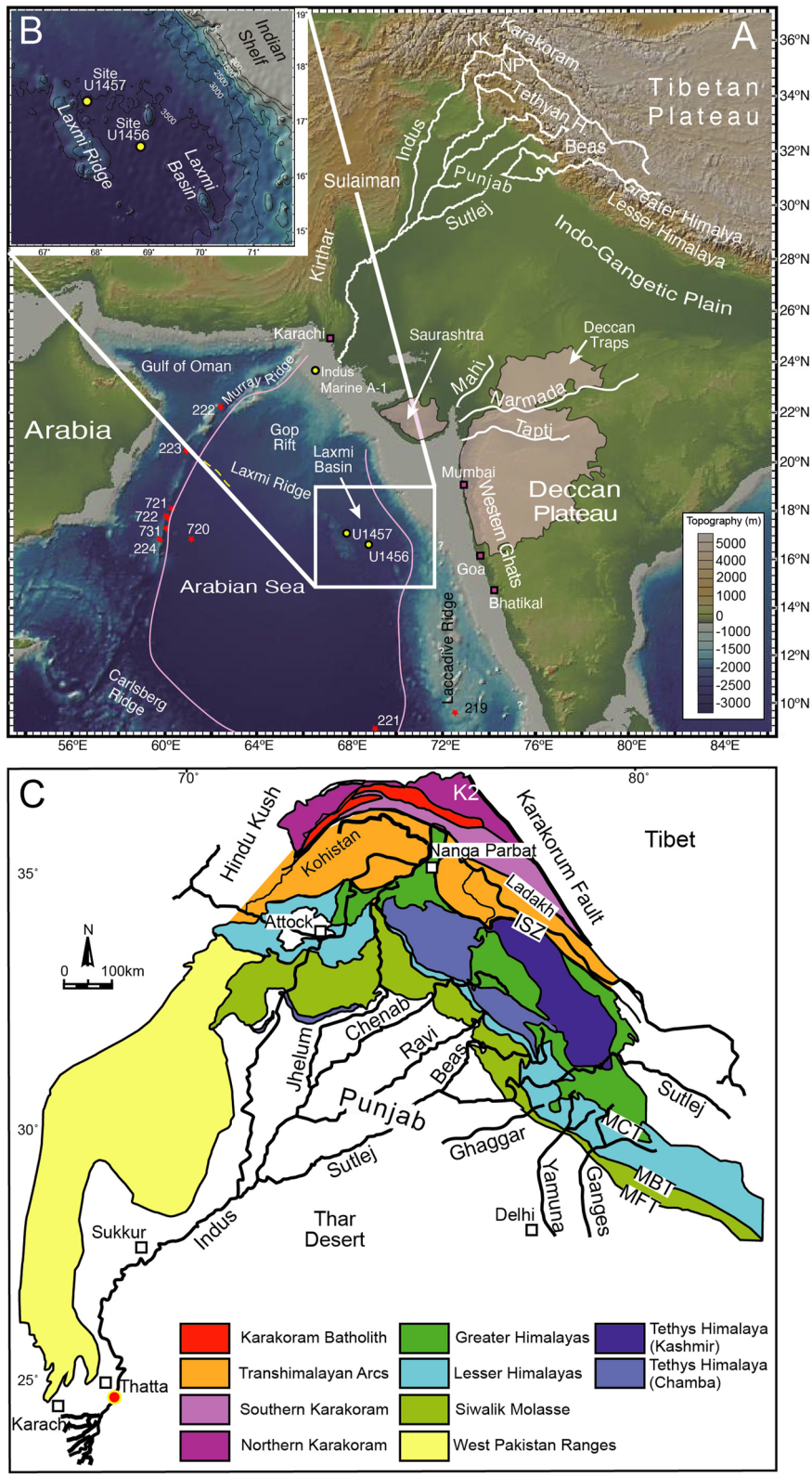
B
Indian Shelf
Site U1457
Site U1456
Laxmi Ridge
Laxmi Basin
A
Tibetan Plateau
KK
Karakoram
NP
Tethyan H.
Indus
Beas
Punjab
Sutlej
Greater Himalaya
Lesser Himalaya
Sulaiman
Kirthar
Indo-Gangetic Plain
Karachi
Saurashtra
Deccan Traps
Gulf of Oman
Indus Marine A-1
Murray Ridge
Mahi
Narmada
Tapti
Arabia
Gop Rift
Laxmi Basin
Laxmi Ridge
Mumbai
Deccan Plateau
Western Ghats
Goa
Bhatikal
Arabian Sea
Laccadive Ridge
Carlsberg Ridge
Topography (m)
5000
4000
2000
1000
0
-1000
-1500
-2000
-2500
-3000
C
Hindu Kush
K2
Karakorum Fault
Tibet
Kohistan
Nanga Parbat
Ladakh
ISZ
Attock
Chenab
Jhelum
Ravi
Beas
Punjab
Sutlej
MCT
MBT
MFT
Ghaggar
Yamuna
Ganges
Delhi
Sukkur
Indus
Thar Desert
Thatta
Karachi
Karakoram Batholith
Transhimalayan Arcs
Southern Karakoram
Northern Karakoram
Greater Himalayas
Lesser Himalayas
Siwalik Molasse
West Pakistan Ranges
Tethys Himalaya (Kashmir)
Tethys Himalaya (Chamba)

Figure 1.

We also compare our sediments with those recovered as drill cuttings from the industrial drill site Indus Marine A-1 located on the Indus shelf (Figure 1a). Because Indus Marine A-1 is located close to the Indus River mouth the source of sediment is more straight-forward, and should be devoid of influence from the Indian Peninsula. This site penetrated into the Middle Miocene (Shuaib, 1982) and drill cuttings have been used to look at the evolving provenance using Nd isotope methods, going back further in time than possible at the IODP sites (Clift & Blusztajn, 2005; Clift et al., 2019). The Indus Marine A-1 drill site is located on the relatively flat continental shelf and is only affected by growth faulting, but has otherwise escaped major tectonic deformation since the breakup of the Arabian Sea, except along its western edge adjacent to the Murray Ridge (Clift, Gaedicke, et al., 2002; Gaedicke et al., 2002). Unfortunately, the recovered sediments from Indus Marine A-1 are fine-grained and not conducive to detrital zircon U-Pb dating. We examined the major element chemistry of the sediments at Indus Marine A-1 for comparison with the more distal drill sites sampled by IODP to establish their Indus provenance. Neodymium isotope data indicate that Indus Marine A-1 sediments were derived from the Indus River, consistent with their proximal location, providing a useful comparison with the deep-water materials (Clift & Blusztajn, 2005).

Determining the provenance of the sediment delivered to the Arabian Sea is facilitated by the leverage of the significant spatial diversity of bedrock ages and lithologies within the Indus drainage basin (Hodges, 2000; Searle, 1996). Geochemical and isotopic differences between bedrock sources are transferred to the eroded sediment and although grains may be altered during the transport process, many of these differences are preserved in the final deposited sediment, allowing us to deconvolve the sources and variations using appropriate proxies. Figure 1c shows the various mountain ranges that comprise the main distinct source regions to the modern Indus River, including the Greater and Lesser Himalaya, as well as the Tethyan Himalaya that lie further north, and that represent the telescoped, passive continental margin of Greater India (Garzanti et al., 1987). This unit is separated by the Indus Suture Zone from magmatic arc rocks of the Transhimalaya and Kohistan (Figure 1c) that were largely emplaced in the Cretaceous and Paleogene (Khan et al., 1997; Rolland et al., 2002). Further north, across the Shyok Suture Zone, lie the Karakoram, the old active margin of continental Eurasia, which also comprises Mesozoic arc rocks that experienced magmatism after India-Eurasia collision, most notably in the form of the Early Miocene Karakoram Batholith (Ravikant et al., 2009; Searle et al., 1989). The Karakoram region was uplifted in response to both compressional tectonics and strike-slip displacement on the Karakoram Fault (Searle & Phillips, 2007). Farther to the west the Hindu Kush mountains are characterized by a similar pre-collisional history as the Karakoram, but subsequently did not experience such dramatic or rapid unroofing (Hildebrand et al., 2001; Zhuang et al., 2018). In addition, the Western Syntaxis of the mountain chain is marked by the Nanga Parbat Massif (Figure 1c), characterized by high-grade metamorphic and igneous intrusive rocks that experienced recent, very rapid exhumation (Zeitler et al., 1989). However, it is unclear exactly when this process began because the rocks now at the surface are very young, although an acceleration after 1.7 Ma has been identified (Crowley et al., 2009). This does not preclude an earlier onset to erosion (Chirouze et al., 2015).

The Greater Himalaya were emplaced along the Main Central Thrust after ~24 Ma, placing them over the Lesser Himalaya (Catlos et al., 2001; Stephenson et al., 2001). These in turn were unroofed and brought to the surface due to motion along the Main Boundary Thrust and associated thrust duplexing (Bollinger et al., 2004; Huyghe et al., 2001). Evidence from the Siwalik Group foreland basin sedimentary strata indicates that the Lesser Himalaya were exposed locally only after 9 Ma and more widely after 6 Ma in Western India (Najman et al., 2009). This is despite the fact that the Nd isotopes at Sites U1456 and U1457 imply that widespread unroofing of the Inner (Crystalline) Lesser Himalaya (ILH) only began at 1.9 Ma (Clift et al., 2019). The Siwalik Group rocks themselves have been up-thrusted and are presently eroding, recycling older sediments back into the river system. However, estimates derived from the incision of terraces in the Nepalese frontal Himalaya imply that the Siwaliks contribute no more than about 15% of the total flux (Lavé & Avouac, 2000). The western edge of the Indus drainage basin is characterized by fold and thrust belts (Sulaiman and Kirthar ranges, Figure 1a), similar to the Siwalik Group in character (Roddaz et al., 2011), but experiencing a more arid climate. Nonetheless, this environment

Figure 1. (a) Shaded bathymetric and topographic map of the Arabian Sea and surrounding area showing the location of the drilling sites considered by this study. Map also shows the major tributary systems of the Indus River, as well as smaller peninsular India rivers and their source mountains. (b) Inset map shows detail of the Laxmi Basin and location of the drill sites considered in this study. Numbered red circles indicate existing scientific boreholes from Deep Sea Drilling Project and Ocean Drilling Program. KK = Karakoram; NP = Nanga Parbat. (c) Geological map of the western Himalaya showing the major tectonic units that are eroded by the Indus River and its tributaries. Map is modified after Garzanti et al. (2005). Rivers as shown in thick black lines. ISZ = Indus Suture Zone, MCT = Main Central Thrust, MBT = Main Boundary Thrust and MFT = Main Frontal Thrust. Thick black line shows the boundary of the Indus drainage, while thinner lines demark the limits of the major Himalayan tributaries. Figure is modified from Clift et al. (2019).

need not limit erosion rates because of the strong erosion associated with occasional flash flooding events in vegetation-poor settings (Molnar, 2001). However, study of heavy minerals in rivers draining these ranges and the lower Indus indicate that their contribution to the net sediment load is minor (Garzanti, Liang, et al., 2020).

Other potential sources of the sediment delivered to the Laxmi Basin include the Precambrian cratonic rocks of peninsular India and associated Gondwanan sedimentary sequences (Mukhopadhyay et al., 2010; Yin et al., 2010), characterized by old (>500 Ma) bedrock zircon U-Pb ages, similar to those found in the Himalaya, especially the ILH. Zircon U-Pb dating, because of its high closure temperature (Hodges, 2003), only records the initial crystallization or high-temperature metamorphism, and thus, does not allow us to exclude such old grains as having been derived from peninsular India rather than the Himalaya. Sediments eroded from the Deccan Plateau, the latest Cretaceous flood basalt province that dominates the Western Ghats, immediately onshore from the drilling area, were erupted around 65 Ma (Courtillot et al., 2000). While such ages would be very distinctive, basalt is characterized by a very low zircon fertility and might not provide significant zircon grains of that age into the adjoining basin. Nd and Sr isotopic evidence suggests enhanced flux of muddy sediments to the Laxmi Basin during interglacial times in the recent geologic past (Khim et al., 2019). Low-resolution apatite fission track and zircon U-Pb studies have so far identified just a single sand at the IODP drill sites that was derived from the Indian peninsula (Zhou et al., 2019).

3. Sedimentology and Stratigraphy

Drilling at Sites U1456 and U1457 penetrated ~1,100 m below the seafloor in both locations, with the basement being reached at Site U1457 (Figure 2) (Pandey et al., 2016b). Drilling at Site U1456 only just penetrated through the MTC, allowing a very short core of undisturbed Middle Miocene sandstone to be recovered (Pandey et al., 2016a). In this study, we followed an age model for both sites based on combining biostratigraphy and magnetostratigraphy (Routledge et al., (2020) (Figure 2). The recovered sequence is not continuous, but rests on the MTC that was emplaced no later than 9.83 Ma (Routledge et al., 2020). The most recent age controls indicate a depositional gap in the preserved section from 1.73 to 2.39 Ma, from 3.92 to 5.59 Ma, and from 8.68 to 9.21 Ma, implying that ~27% of the time since 9.83 Ma is not represented in the section. These hiatuses likely reflect autocyclic processes, such as lobe switching on the submarine fan. Given the fine-grained nature of parts of this section, not all the sediments are suitable for zircon dating, resulting in a detrital zircon record spanning four discontinuous sections.

Ages of individual samples are calculated assuming linear sedimentation between the dated points (Table 1). Uncertainties are likely around 100 ky for depositional ages, and therefore we report zircon U-Pb ages to one decimal place. At Site U1456 the sediments are relatively mud-rich, but with a number of silt and fine sand turbidite interbeds at 460–730 mbsf (meters below seafloor; Figure 2a), which are overlain by a sequence of mud and carbonate-rich sediments. A thick, sand-rich package was recovered between 360 and 140 mbsf that was originally interpreted as a submarine fan lobe (Pandey et al., 2016a), but is now considered as channel fill (Andò et al., 2020). Above this sand-rich package, the section is dominated by mud and carbonate, interpreted as the product of hemipelagic sedimentation. Site U1457 is characterized by much lower proportions of sand, reflecting its location on the flanks of the Laxmi Ridge. However, a sand-rich interval between 670 and 810 mbsf is overlain by a carbonate and mud-rich interval between 600 and 670 mbsf. More sand-rich beds were encountered between 470 and 600 mbsf. As at Site U1456, sediments shallower than 200 mbsf at Site U1457, are mud and carbonate-rich (Figure 2). The coarse-grained intervals are again re-interpreted as channel-fill deposits (Andò et al., 2020). The sandy sediments are interpreted as having been deposited by turbidity currents, with the muddy sediments representing hemipelagic intervals between depositional events. Changes in grain size might be driven by changes in erosional power in the source regions, the stream power of the river, or by changes in sea level, but could also reflect avulsion of the main depositional channels and lobes in and out of Laxmi Basin and the main part of the Arabian Sea located toward the West. Such autocyclic behavior is commonly observed in submarine fans (Deptuck et al., 2008; Shanmugam & Moiola, 1991).

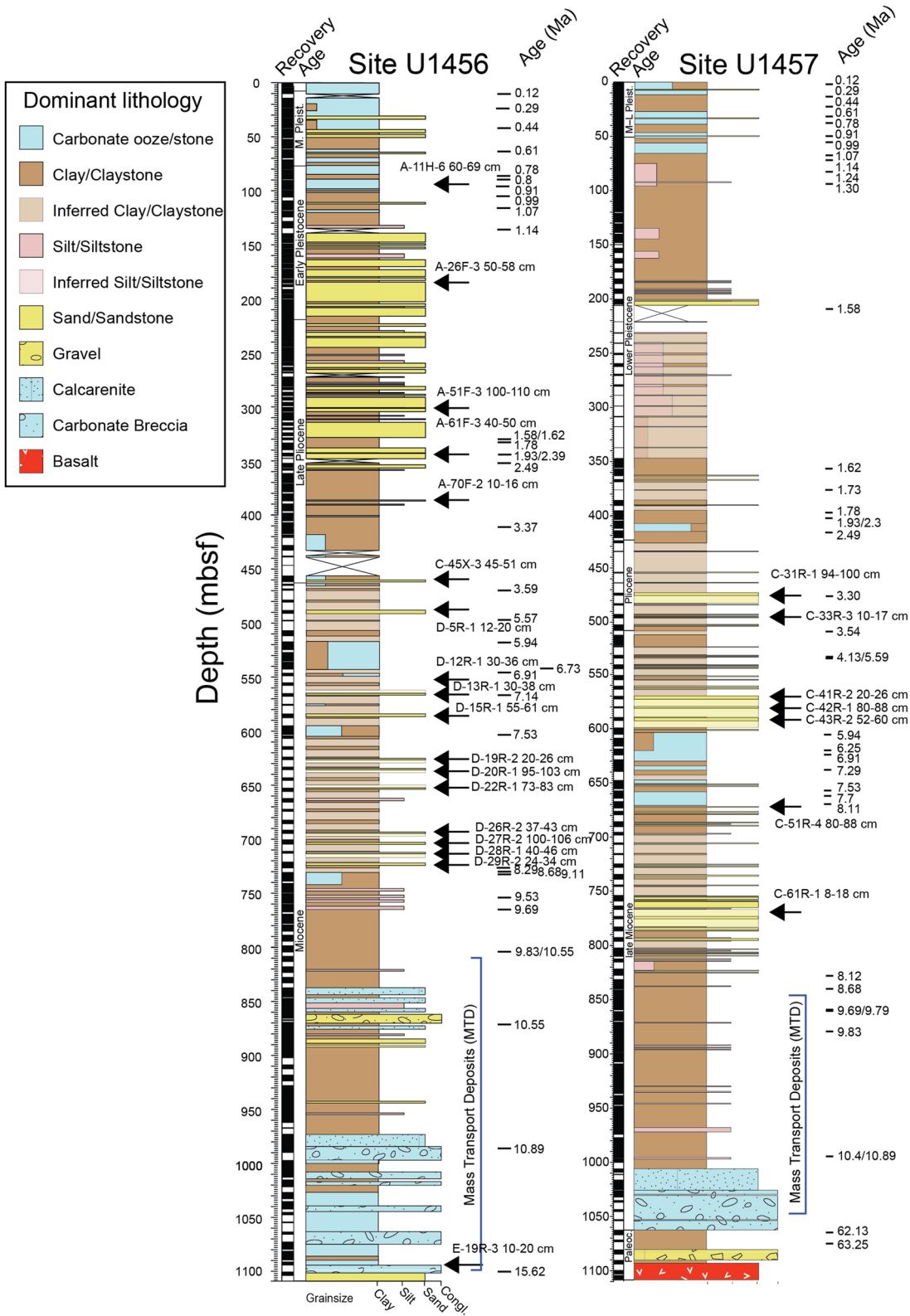

Figure 2. Simplified lithologic logs of the two drill sites considered in this study. Black arrows show the location of the samples analyzed. Modified from Pandey et al. (2016c). Pale shaded intervals show inferred lithologies based on small amounts of recovered core. Because induration is progressive and there is no sharp division, we make no attempt to distinguish between sediments and indurated rocks. Numerical ages are from Routledge et al. (2020).

Table 1
Major Elements Major Elements Geochemical Analysis of the Samples Considered in This Study

Sample	Age (Ma)	SiO_2 (%)	Al_2O_3 (%)	CaO (%)	Fe_2O_3 (%)	MgO (%)	Na_2O (%)	K_2O (%)	P_2O_5 (%)	MnO (%)	TiO_2 (%)	Ba (ppm)	Zr (ppm)	Sc (ppm)	Mean Grain Size (μm)	In Clift et al. (2019)
U1456A-11H-6 60-69 cm	0.95	56.53	14.00	3.14	8.68	2.86	1.98	1.96	0.21	0.04	1.44	323.5	174.4	244.1	31.9	Yes
U1456A-26F-3 50-58 cm	1.26	71.08	12.15	1.50	3.80	1.52	1.99	2.47	0.12	0.04	0.57	345.1	214.9	141.3	125.1	
U1456A-51F-3 100-110 cm	1.56	71.69	12.23	1.54	3.81	1.66	2.10	2.52	0.13	0.04	0.60	399.7	216.1	151.4	137.4	Yes
U1456A-61F-3 40-50 cm	2.46	72.28	11.36	1.87	3.33	1.40	2.03	2.22	0.11	0.04	0.54	321.7	223.8	158.3	142.2	Yes
U1456A-70F-2 10-16 cm	3.07	60.92	16.16	1.06	5.87	2.69	1.37	3.23	0.12	0.04	0.80	491.7	168.7	130.5	13.5	Yes
U1457C-31R-1 94-100 cm	3.19	62.19	15.57	1.24	5.70	2.59	1.91	3.67	0.16	0.05	0.74	541.3	177.2	151.7	46.5	
U1457C-33R-3 10-17 cm	3.39	66.93	13.55	1.38	4.72	2.31	1.89	2.74	0.12	0.05	0.71	409.6	142.2	147.2	132.1	Yes
U1456C-45X-3 45-51 cm	3.58	64.81	14.33	1.13	5.25	2.39	1.59	2.87	0.10	0.04	0.73	423.6	138.9	132.1	60.3	
Indus Marine A1-1620	3.60	58.33	15.42	1.58	6.89	3.21	1.36	3.09	0.20	0.06	0.80	4954.7	193.6	15.1	17.2	
Indus Marine A1-2200	5.16	56.88	13.97	2.90	8.90	2.59	1.35	2.68	0.20	0.09	0.70	1368.1	229.2	13.6	14.0	
U1456D-5R-1 12-20 cm	5.70	61.90	15.40	1.11	5.75	2.57	1.50	3.05	0.13	0.04	0.80	473.8	219.7	132.5	29.8	Yes
U1457C-41R-2 20-26 cm	5.76	64.85	14.74	1.20	5.28	2.37	1.57	2.73	0.14	0.04	0.77	413.8	210.2	135.0	47.1	
U1457C-42R-1 80-88 cm	5.81	70.30	11.81	1.56	3.51	1.51	2.02	2.21	0.12	0.04	0.53	393.4	195.3	168.4	69.1	
U1457C-43R-2 52-60 cm	5.87	65.58	14.25	1.27	4.99	2.30	1.69	2.93	0.13	0.04	0.74	395.4	193.8	141.4	103.5	Yes
Indus Marine A1-3180	6.93	53.46	14.16	1.96	7.23	2.52	1.13	2.68	0.19	0.05	0.74	32834.9	192.8	13.2	13.7	
U1456D-12R-1 30-36 cm	7.03	67.20	13.36	2.05	4.70	2.24	2.06	2.37	0.14	0.05	0.67	318.5	170.0	187.9	94.6	
U1456D-13R-1 30-38 cm	7.13	63.84	13.55	1.60	4.84	2.37	1.95	2.62	0.12	0.04	0.68	336.2	156.7	163.8	99.1	Yes
U1456D-15R-1 55-61 cm	7.39	65.51	13.66	1.62	4.79	2.33	1.92	2.61	0.13	0.04	0.69	331.1	169.2	165.6	43.3	
U1456D-19R-2 20-26 cm	7.66	64.67	14.54	1.53	5.09	2.39	1.97	2.97	0.16	0.04	0.71	398.3	175.2	169.4	64.0	
U1456D-20R-1 95-103 cm	7.72	63.54	14.45	1.36	4.86	2.45	1.64	2.85	0.15	0.04	0.75	304.9	190.6	145.2	32.3	
U1456D-22R-1 73-83 cm	7.84	62.40	15.48	1.31	5.42	2.63	1.55	2.94	0.14	0.04	0.78	338.4	170.0	146.3	27.2	Yes
U1456D-26R-2 37-43 cm	8.08	67.41	12.96	1.66	4.51	2.28	2.12	2.37	0.14	0.04	0.64	348.4	208.4	166.1	71.8	
U1457C-51R-4 80-88 cm	8.11	66.13	13.89	1.43	4.75	2.31	1.85	2.66	0.12	0.04	0.70	311.3	153.7	154.2	63.0	
U1457C-61R-1 8-18 cm	8.12	67.73	13.23	1.56	4.65	2.27	1.97	2.37	0.13	0.04	0.62	309.6	151.3	160.6	75.3	
U1456D-27R-2 100-106 cm	8.15	62.63	15.15	1.16	5.43	2.69	1.44	2.79	0.16	0.04	0.82	325.5	162.1	135.6	23.4	
U1456D-28R-1 40-46 cm	8.20	62.57	14.94	1.18	5.28	2.58	1.59	2.72	0.16	0.04	0.75	362.7	187.9	141.2	23.5	
U1456D-29R-2 24-34 cm	8.27	62.11	15.26	1.13	5.38	2.68	1.50	2.81	0.14	0.04	0.78	352.3	181.0	133.2	25.5	Yes
Indus Marine A1-3960	8.29	57.99	14.60	2.10	8.99	2.69	1.65	2.84	0.19	0.06	0.76	715.1	228.2	13.5	16.2	
Indus Marine A1-4180	8.68	57.30	14.68	1.91	8.27	2.72	1.53	2.75	0.18	0.06	0.75	1145.3	224.7	13.1	15.3	
Indus Marine A1-4840	9.83	59.23	15.59	1.22	7.63	2.70	1.54	2.95	0.18	0.05	0.77	671.3	202.5	14.3	14.1	
Indus Marine A1-4940	10.00	60.71	15.24	0.88	6.46	2.60	1.59	2.87	0.17	0.05	0.77	7977.0	222.6	13.5	13.9	
Indus Marine A1-5360	10.72	57.44	15.63	1.46	8.77	3.11	1.31	2.80	0.21	0.06	0.83	686.6	203.3	14.6	12.8	
Indus Marine A1-5920	11.67	56.44	16.72	0.62	7.96	2.96	1.18	3.28	0.16	0.05	0.85	532.3	185.7	15.5	10.4	
Indus Marine A1-6360	12.35	57.18	16.77	0.71	7.15	3.08	1.16	3.12	0.16	0.04	0.86	534.6	191.3	15.7	12.0	
Indus Marine A1-6460	12.51	60.96	16.20	0.72	7.15	2.96	1.23	2.87	0.17	0.04	0.81	498.5	177.5	14.2	9.9	
Indus Marine A1-6680	12.86	58.50	18.08	3.68	6.92	3.42	1.19	3.05	0.18	0.04	0.84	420.1	178.5	15.1	10.3	
Indus Marine A1-6890	13.19	58.98	16.90	0.84	7.04	3.11	1.06	3.04	0.17	0.04	0.87	488.8	192.4	15.3	10.7	
Indus Marine A1-7090	13.50	58.76	16.27	0.62	7.05	3.13	0.79	2.96	0.16	0.04	0.88	420.8	206.2	14.6	12.0	
Indus Marine A1-7190	13.66	59.46	15.38	0.66	8.12	2.88	0.90	2.72	0.16	0.05	0.83	763.8	223.4	13.9	11.9	

Table 1
Continued

Sample	Age (Ma)	SiO_2 (%)	Al_2O_3 (%)	CaO (%)	Fe_2O_3 (%)	MgO (%)	Na_2O (%)	K_2O (%)	P_2O_5 (%)	MnO (%)	TiO_2 (%)	Ba (ppm)	Zr (ppm)	Sc (ppm)	Mean Grain Size (μm)	In Clift et al. (2019)
Indus Marine A1-7400	13.99	58.12	16.08	0.64	7.82	3.06	0.93	3.08	0.15	0.04	0.84	520.6	197.6	15.6	11.7	
Indus Marine A1-7500	14.14	59.07	16.23	0.58	7.58	3.06	0.69	3.04	0.15	0.04	0.88	518.3	225.1	15.6	10.4	
Indus Marine A1-7620	14.33	58.48	16.12	0.57	7.17	3.05	0.82	2.99	0.16	0.04	0.86	483.7	224.5	15.7	12.0	
Indus Marine A1-7720	14.49	58.75	16.42	0.74	7.06	3.20	0.87	3.15	0.15	0.04	0.87	454.1	216.7	14.9	11.7	
Indus Marine A1-7820	14.64	57.76	16.12	0.59	7.00	3.07	0.88	2.91	0.15	0.04	0.86	530.2	215.8	14.8	10.8	
Indus Marine A1-8040	14.99	58.43	16.32	0.58	7.07	3.12	0.83	3.14	0.15	0.04	0.87	465.6	206.4	15.4	10.7	
Indus Marine A1-8140	15.15	58.48	16.47	0.53	7.34	3.20	0.84	3.15	0.16	0.04	0.87	359.5	214.8	14.6	11.4	
Indus Marine A1-8240	15.30	57.92	16.05	0.79	7.01	3.34	0.81	2.99	0.17	0.04	0.88	366.9	224.7	16.4	12.5	
Indus Marine A1-8340	15.46	57.50	15.41	0.72	6.88	3.23	0.80	2.88	0.15	0.04	0.84	15154.2	226.9	15.2	13.6	
U1456E-19R-3 10-20 cm	15.62	65.14	13.85	1.15	4.97	2.72	1.70	2.68	0.15	0.04	0.69	315.8	182.4	141.7	53.1	Yes
Indus Marine A1-8450	15.63	53.35	11.98	0.77	6.18	2.37	0.72	2.10	0.12	0.03	0.67	67660.3	207.5	11.8	17.5	
Indus Marine A1-8650	15.94	39.71	7.64	0.55	3.87	1.29	0.53	1.25	0.10	0.02	0.44	94222.9	225.8	8.5	16.9	
Indus Marine A1-8950	16.42	48.08	9.12	0.72	4.51	1.64	0.87	1.51	0.11	0.03	0.55	95848.9	278.7	7.4	14.5	
Indus Marine A1-9170	16.76	52.48	11.88	0.70	6.54	2.42	0.83	2.15	0.14	0.04	0.66	74337.3	187.9	10.4	20.9	

Note. Depositional ages are expressed to two decimal places assuming linear sedimentation between age control points and to emphasize which samples are older and younger when they were deposited at a similar time, although the actual uncertainties are greater than that.

4. Methods

4.1. Major Element Analyses

Bulk sediment samples were analyzed for their major element contents by Inductively Coupled-Plasma Emission Spectrometry at Boston University (BU), USA. Sediment samples were decarbonated with acetic acid, washed with distilled and deionized water (9–12 megaohms), and hand powdered at Louisiana State University (LSU) before total fusion preparation at BU. Glass beads for each sample were made in a muffle furnace under 1,050°C by fusing 100 ± 0.5 mg of sample mixed with 400 ± 0.5 mg lithium metaborate ($LiBO_2$). The melted mixture was then dissolved in 5% HNO_3, sonicated, manually shaken until no visible grains were observed, and further diluted for analysis (Dunlea et al., 2015). Precision for all elements was better than 1% of the measured value, and accuracy was confirmed by repeated analyses of International Standard Reference Materials (Basalt, Hawaiian Volcano Observatory, BHVO-2) (Wilson, 1997). Results of the geochemical measurements are shown in Table 1.

4.2. Grain Size Analysis

For quantitative grain size analysis, samples were prepared using standard procedures as described by Howell et al. (2014). We put a small amount of sample into a cleaned 50 ml plastic centrifuge tube and added 5–7 ml of sodium phosphate solution. The tube was capped and vortexed to deflocculate clay-sized sediment and separate organic particles. Each sample was poured through an 850 μm sieve and funneled into a 15 ml glass test tube. After centrifuging and removing the clear supernatant, 2–3 ml of sodium phosphate and 5 ml of 30% H_2O_2 were added. Tubes were vortexed again and then put into a hot bath that was heated to 70°C. This step required persistent monitoring to prevent loss of reactant by spraying it with acetone until the reaction is stabilized. Reactants then sat overnight to completely oxidize any organic matter. Reacted supernatant was removed, and 5 ml of sodium phosphate was added. These treated samples were then rinsed with deionized water, transferred into clean 50 ml plastic centrifuge tubes, and topped up with sodium phosphate into a sample solution of up to 40 ml. Samples were vortexed again prior to grain size analysis. Grain size analysis was conducted on a Beckmann Coulter LS13 320 laser diffraction particle size analyzer at LSU. The obscuration of all running samples in the aqueous liquid module was between 8% and 12%. Result of the analysis are provided in Table S1.

4.3. Zircon U-Pb Dating

Detrital zircon U-Pb geochronology has become a powerful and widely employed tool for discerning provenance in siliciclastic sedimentary systems. The methodology is based on the concept that different bedrock source rocks are characterized by distinct and/or different age populations of zircons. However, a zircon budget is not the same as an eroded rock budget because of differences in the relative fertility of zircon in bedrock sources. Zr concentrations have been used as a proxy for the relative abundance of zircons in sediment (Amidon et al., 2005), but the reliability of this approach has recently been questioned (Malusà et al., 2016). Malusà et al. (2016) developed a method using mineralogy and density data from the sediment to infer the fertility of the source bedrock. Unfortunately, this approach is not practical for this work because the sample sizes available from IODP were small (<50 cm^3) so that all the material had to be processed for zircon extraction and even required amalgamating neighboring samples in some cases to generate enough data for statistically meaningful results. We use previously published geochemical data from modern rivers as a guide to zircon fertility because these data already exist and we cross checked this prediction against other provenance methods to assess its credibility. Our erosion budgets are however largely zircon-based, and not necessarily the same as bulk sediment.

Zircon is a robust mineral and its grains do not generally experience significant physical abrasion during transport unless they had previously accumulated major radiation damage. Although metamict zircons may experience some dissolution, unleached ZrO_2 residue produced during incongruent leaching conditions acts as an effective dissolution barrier and this is not considered an important factor (Tromans, 2006). Hence, zircon can undergo multiple episodes of recycling and redeposition. Although the concentration of zircon in any given sediment can be affected by hydrodynamic sorting, this process may not be a strong influence on the resulting detrital age spectra unless there is a relationship between grain size and crystallization age, which we investigate below. Work on Yangtze River sediments indicates that the typical grain size range analyzed using LA-ICP-MS technology is representative of the overall population in the sediment without a bias related to grain size (Yang et al., 2012). Detrital zircon U-Pb dating has been widely applied in provenance studies in the Western Himalaya because of the large differences in zircon U-Pb age spectra between the various source terrains described above. Furthermore, studies of the modern Indus River documented a close correlation between the modern zircon U-Pb age spectra and the bedrock sources, albeit one implying focused erosion in several sub-basins (Alizai et al., 2011; Zhuang et al., 2018). Several studies have also used detrital zircon dating to investigate the provenance of Siwalik Group foreland basin sedimentary rocks (Baral et al., 2015; Bernet et al., 2006; DeCelles et al., 2004; Zhuang et al., 2015) and Quaternary sediments in the delta and offshore (Clift, Giosan, et al., 2008; Li et al., 2019), allowing evolving erosion patterns to be reconstructed.

Standard mineral separation with heavy liquids was enhanced with the methods of Donelick et al. (2005) to recover all possible grain sizes and minimize the potential loss of smaller grains through the use of a water table. Zircon grains were sprinkle-mounted onto double-sided tape on 1″ acrylic discs and analyzed at random using depth-profiling LA-ICP-MS U-Pb geochronology (Marsh & Stockli, 2015), to systematically recover the youngest ages and multiple ages from individual zircons. Although this method differs from the more common analysis of polished grain interiors there is no indication that this profiling approach yields results that differ significantly from earlier work, including work done in the Himalaya (Colleps et al., 2019). For each sample at least 120 zircons were analyzed to obtain provenance datasets that resolve all components that comprise >5% of the total population (Vermeesch, 2004).

The analyses were completed using a PhotonMachine Analyte G.2 Excimer laser (30 μm laser spot size) with a large-volume Helex sample cell and a Thermo Element2 ICP-MS using procedures described in Hart et al. (2016) at the UTChron facilities of the Jackson School of Geosciences at the University of Texas at Austin. GJ1 was used as the primary reference standard (Jackson et al., 2004), with a secondary in-house zircon standard (Pak1 with a TIMS $^{206}Pb/^{239}U$ age of 43.0 Ma). The data from the analyses were then reduced using the Iolite data reduction software VizualAge (Paton et al., 2011; Petrus & Kamber, 2012). For analyzed detrital zircons, the $^{206}Pb/^{238}U$ age was used for grains younger than 850 Ma and the $^{207}Pb/^{206}Pb$ age was used for grains older than 850 Ma (Gehrels et al., 2008). All ages reported use 2σ absolute propagated uncertainties. $^{207}Pb/^{206}Pb$ ages are less than 30% discordant, and $^{206}Pb/^{238}U$ ages are less than 10% discordant (Gehrels et al., 2011).

The discordance reported is calculated with the $^{206}Pb/^{238}U$ and $^{207}Pb/^{235}U$ ages if <850 Ma and the $^{206}Pb/^{238}U$ and $^{207}Pb/^{206}Pb$ ages if >850 Ma. Although some studies have recommended an older crossover at 1.5 Ga between

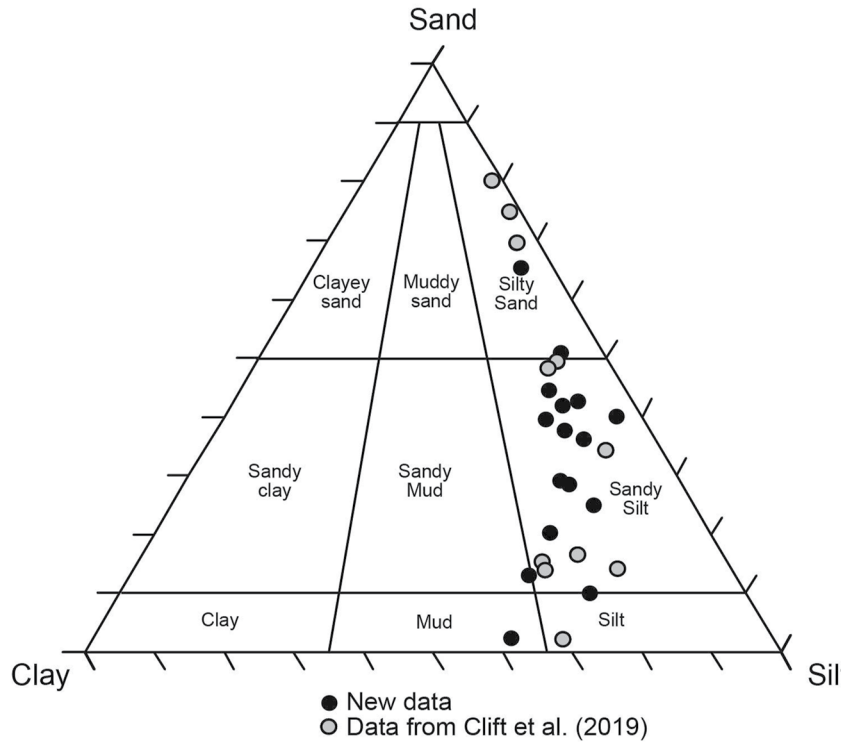

Figure 3. Grainsize range of all samples analyzed for U-Pb zircon dating from the Laxmi Basin shown on the scheme of Folk (1974). Samples are marked to show those published by Clift et al. (2019), rather than presented new here (Table S1). Note the dominance of silty sand and sandy silt in the analyzed samples.

the $^{206}Pb/^{238}U$ and $^{207}Pb/^{235}U$ ages and the $^{206}Pb/^{238}U$ and $^{207}Pb/^{206}Pb$ ages (e.g., 1.5 Ga (Spencer et al., 2016)), in our specific data set this would lead to drastic culling of grains with precise $^{206}Pb/^{207}Pb$ ages with discordant $^{206}Pb/^{238}U$ ages, or unacceptable smearing and loss of age mode definition between 800–1,500 Ma for most of our samples. For example, selecting a 1,500 Ma crossover cutoff and a 20% discordance filter would result in the loss of 80% of the data between 850 and 1,500 Ma making the data bad as provenance proxies. The 850 Ma crossover was chosen in accordance with the approach of Spencer et al. (2016) and Marsh et al. (2019). The data are reported in Table S2.

When accurately and precisely dating a geological event, high concordance and maximum precision is a requirement but when assigning grains to age modes for provenance work the emphasis is on high numbers of grains rather than on slightly higher precision to improve the statistical reliability. The appropriate level of discordance filter needs to be determined for each data set in light of the goals of the study and the complexities encountered. If a study yields a mix of Phanerozoic and Archean ages, and the relative proportions of these ages are important, a generous (e.g., 30%) discordance cutoff is appropriate so that most Precambrian ages are retained (Gehrels, 2012).

5. Results

5.1. Grain-Size of Sediments

Both the new samples processed here and those from the earlier study (Clift et al., 2019) were assessed using the classification scheme of Folk (1974) (Figure 3), and range from silty sand to silt and mud. The grain size variation in single samples can be better assessed by plotting the proportion of each grain size fraction as a spectrum (Figure 4). We see generally good sorting within individual samples (positive kurtosis, mean of 1.83) and a negative skew (mean −1.39), meaning a dominance of the finer grain sizes and a tail of coarser grains comprising a diminishing proportion of the sediment. This is especially true for the coarsest grained sediments (Table S1). The vast majority of the sediment considered here is classified as fine sand to silt, with only small amounts of

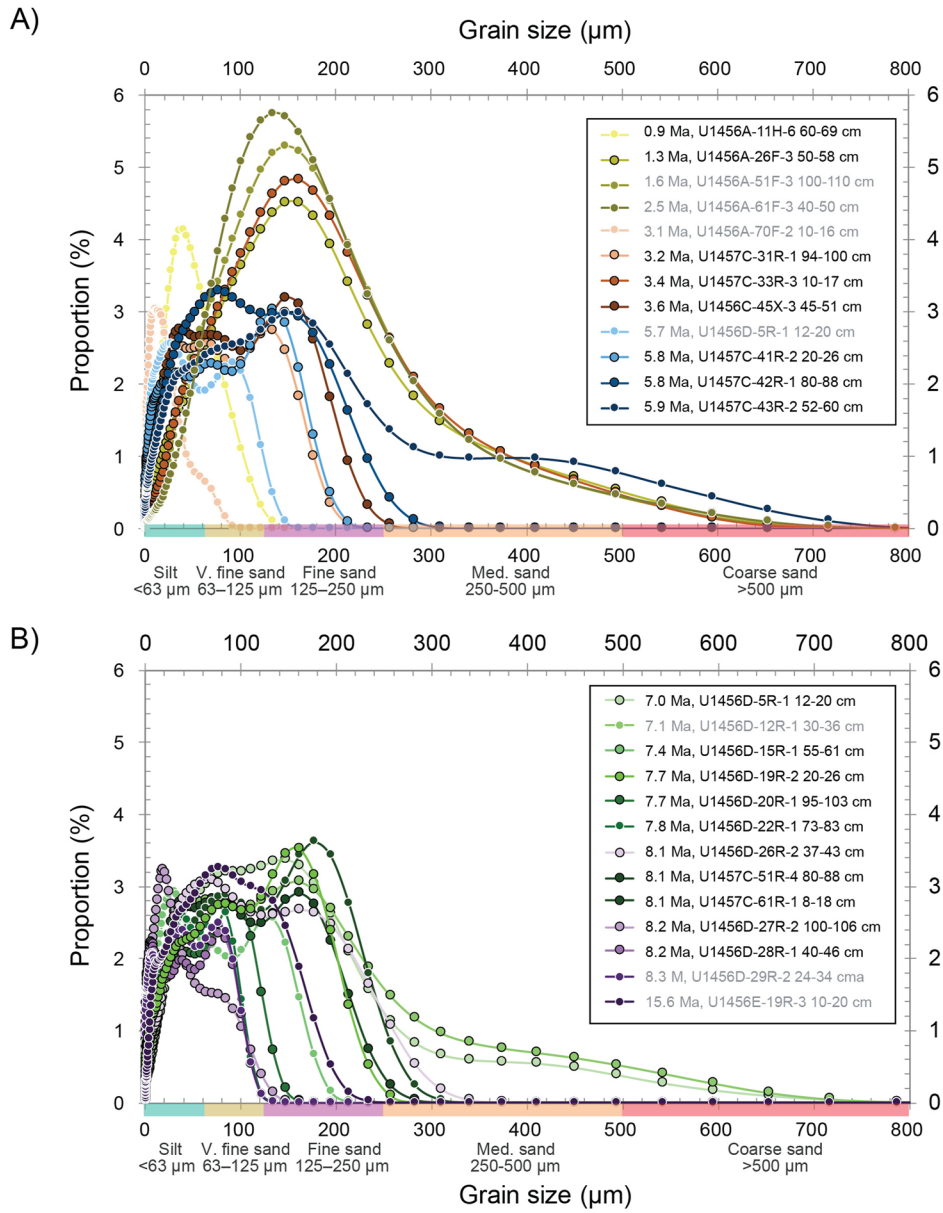

Figure 4. Detailed grain size spectra showing the range of sizes of the different samples considered within this study. Most of the sediment is fine sand to coarse silt in size and typically shows a coarse-skewed. (a) Samples younger than 7 Ma, (b) samples older than 7 Ma. Samples are marked to show those published by Clift et al. (2019) (gray text labels and white ringed symbol), rather than presented new here (Table S1) (black text labels and black ringed symbol).

medium and coarse sand in a minority of samples; three from Site U1456 dated at 1.9–1.3 Ma and one from Site U1457 dated at 3.0 Ma. Three of the new samples contain significant volumes of medium and even coarse sand (deposited at 3.4, 7.0, and 7.3 Ma). The spot size of the laser used for the U-Pb dating means that grains smaller than ~30 μm were not considered in this study. Depending on the sample this represents a wide range of the total sediment load. Only 9% of Sample U1456A-51F-3, 100–110 cm was less than 30 μm, while 89% of Sample U1456A-70F-2, 10–16 cm is smaller than that threshold.

5.2. Bulk Sediment Chemistry

The general geochemical character of the sediments can be seen on a CN-A-K ternary diagram (Fedo et al., 1995, Figure 5a). The IODP samples plot in an array with a Chemical Index of Alteration (CIA) of ~65–73 (Nesbitt

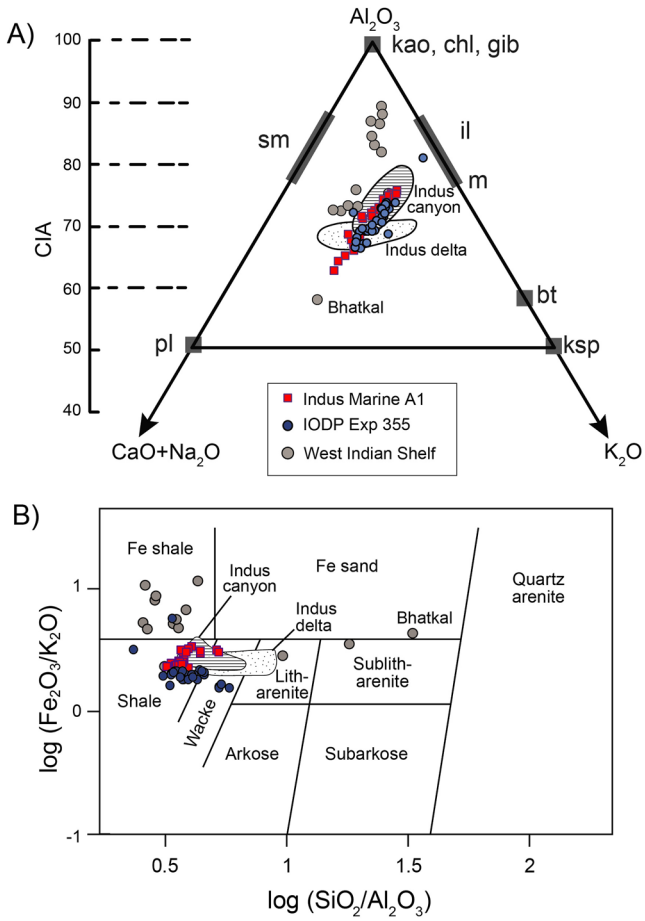

Figure 5. (a) Geochemical signature of the analyzed samples illustrated by a CN-A-K ternary diagram (Fedo et al., 1995). CN denotes the mole weight of Na_2O and CaO* (CaO* represent the CaO associated with silicate, excluding all the carbonate). A and K indicate the content of Al_2O_3 and K_2O respectively. Samples closer to A are rich in kaolinite, chlorite and/or gibbsite (representing by kao, chl, and gib). CIA values are also calculated and shown on the left side, with its values are correlated with the CN-A-K. Samples from the delta have the lowest values of CIA and indicates high contents of CaO and Na_2O and plagioclase. Abbreviations: sm (smectite), pl (plagioclase), ksp (K-feldspar), il (illite), and m (muscovite). (b) Geochemical classification of sediments from this study as well as those from the Indus delta (Clift et al., 2010), Indus Canyon (Li et al., 2018), and western Indian shelf (Kurian et al., 2013) following the scheme of Herron (1988).

et al., 1980). They form a roughly linear array trending toward the illite end member and suggestive of its progressive involvement as the primary mineral breakdown product. The Laxmi Basin samples can be compared with sediments from the Quaternary Indus delta (Clift et al., 2010), Indus Canyon (Li et al., 2018), the Indus Marine A-1 borehole, as well as modern sediments from the western Indian shelf and slope between the Saurashtra peninsula and Bhatikal (Kurian et al., 2013) (Figure 1). Rivers south of Bhatikal have a different composition and are unlikely to be sources to the Laxmi Basin sites.

The Laxmi Basin sands have very similar bulk compositions to the Quaternary Indus Canyon and delta, as well as the Indus Marine A-1 samples (Figure 5a), but plot below or to the right of the array of the western Indian shelf sediments. Only the shelf sample taken near Bhatikal (the southernmost shelf sample that overlies the Precambrian crystalline basement of India, rather than the Deccan Traps), plots below the Laxmi Basin sediments, with a lower CIA value. This plot confirms that the analyzed sands have little in common with material eroded from peninsular India and appear consistent with an Indus River origin. Likewise, the sediments plot close to the Quaternary Indus sediments and those of Indus Marine A-1 on the discrimination diagram of Herron (1988) (Figure 5b). The IODP samples plot with slightly lower Fe_2O_3/K_2O values compared to the proximal sediments. The Laxmi Basin sediments form an array defined as shales and wackes, while the western Indian shelf sediments fall into the Fe shale, litharenite, sublitharenite, and Fe sand fields.

We further assessed whether grain size has any impact on zircon concentration by plotting Zr against median grain size (Figure 6a). Although the original source characteristics and hydrodynamic sediment sorting might be expected to concentrate zircons in certain size fractions this does not appear to be a significant factor within the range of grain sizes considered here, although it is likely to be the case when considering the total range of sediments recovered at this site (Andò et al., 2020). Coupled heavy mineral studies and geochemical data from Plio-Pleistocene deposits confirm that zircon is concentrated in the sandy turbidite channel fills that comprise the thicker, meter-scale units (Andò et al., 2020). It is these deposits that are the focus of this work given the need for significant sediment volumes to yield sufficient grains, and the limits on sample size imposed by IODP. Furthermore, we note that Zr and thus zircon contents show a weakly defined temporal trend to lower values from 18 Ma to the present day, although zircon-yielding sediments are found throughout the section.

5.3. Detrital Zircon U-Pb

We examined the range of zircon U-Pb ages using a kernel density estimate diagram to characterize the modal age spectra of individual samples and to assess similarities between different sampled sediments and potential source regions (Figure 7). All of the sediments analyzed in this study show a significant zircon U-Pb component younger than 200 Ma. In addition, we see major components dated at 350–1,250 and 1,500–2,300 Ma. The abundance of these older age components overall increases with decreasing sample depositional age. The 350–1,250 Ma age component increases in all sediment samples dated at 5.9 Ma or younger compared to the older sediments. A particularly prominent age mode at ~1,800 Ma first occurs in sediments deposited at 3.4 Ma and becomes extremely prominent in all samples younger than 1.9 Ma. This age mode has also been observed in the modern sediment from the Indus River mouth (Clift et al., 2004).

Examining the <200 Ma zircon U-Pb ages in detail, we see that the vast majority of grains are younger than 120 Ma, with prominent age peaks at 100–120 and 40–70 Ma (Figure 8). In the youngest samples, especially those deposited after 3.0 Ma, we see another age mode at ~20 Ma, although this is also seen in the sample dated

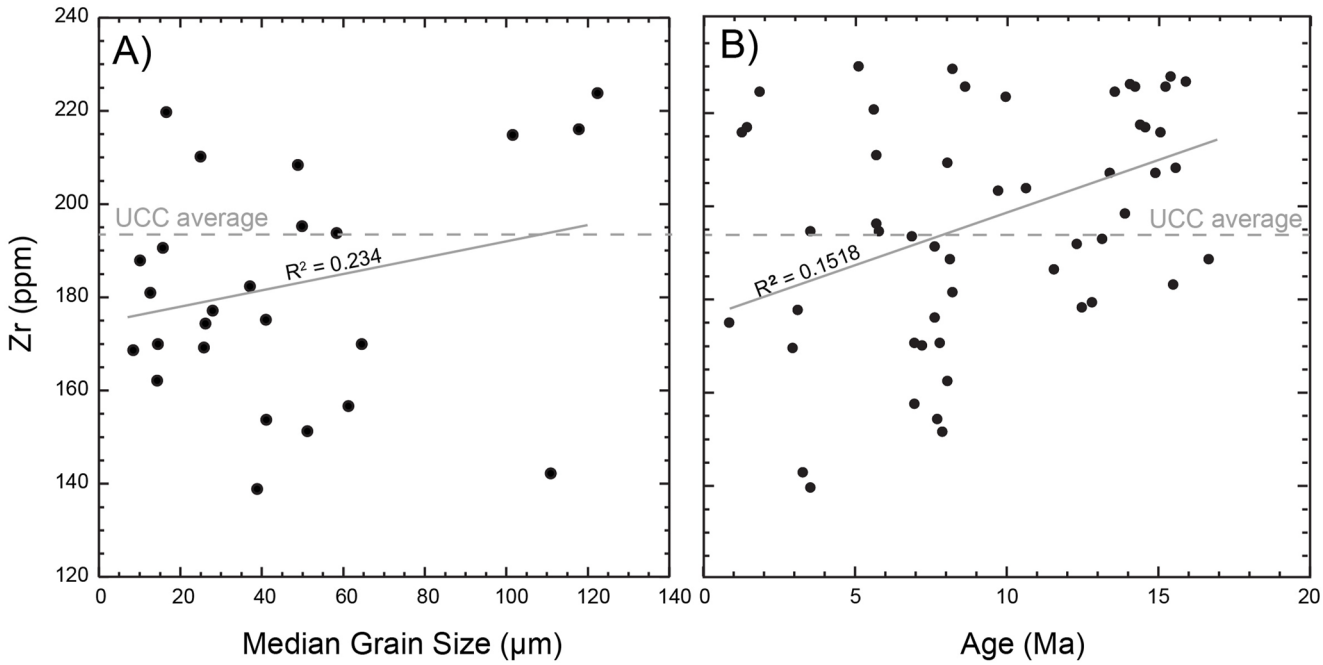

Figure 6. (a) Cross plot of Zr concentration against median sample grain size. No strong correlation is observed. (b) Cross plot of Zr concentration against deposition age showing a weak negative correlation.

at 5.8 Ma. One sample deposited at 3.2 Ma differs in its <200 Ma age spectra from the other samples as it is characterized by a prominent age peak at 100–120 Ma, with a general lack of other younger zircon grains.

6. Discussion

6.1. Major Element Compositions

Major element discrimination diagrams (Figure 5) suggest that the Laxmi Basin sediments are most similar to deposits found in the Quaternary and modern Indus River/delta/canyon, as well as the older sedimentary rocks from Indus Marine A-1 (Figure 5). However, they are distinctly different from sediments sampled from the modern western Indian shelf that are largely derived from the Deccan Plateau and underlying units (Kurian et al., 2013). Geochemical data indicate that the Laxmi Basin sediments analyzed in this study most likely originated from the Indus River mouth. Such an interpretation is consistent with heavy mineral studies that imply a Himalayan origin for the turbidite sediments from these sites (Andò et al., 2020), with limited influence from western India only seen within the Pleistocene hemipelagic nannofossil oozes at the top of the section (Garzanti, Andò, & Vezzoli, 2020; Zhou et al., 2019).

We assessed the overall geochemical characteristics of the sediments by plotting the major element composition of each sample normalized to the upper continental crust (UCC; Figure 9) (Taylor & McLennan, 1995). Most of the samples display a relatively uniform topology in these diagrams and are broadly similar to both post-LGM sediments from the Indus Delta (KB-40-4), the Holocene delta (TH-10-1) and the modern Indus River (Thatta TH-1). Most of the samples show a similar major element composition compared to the UCC, with a consistent enrichment in TiO_2, suggestive of a higher content of Ti-bearing heavy minerals (e.g., rutile, anatase, brookite, ilmenite, and titanite). This enrichment is particularly strong in the 0.9 Ma sample which apatite fission track data indicate to have a unique provenance (Zhou et al., 2019). There are also relative depletions in CaO and Na_2O, as well as P_2O_5, implying both a lower plagioclase and apatite content relative to the UCC. Relative depletion in CaO is strongest in the modern river mouth sediment and weakest in the post-glacial delta sediments, with the fan sediments plotting between these extremes. The systematically lower abundance of plagioclase and apatite likely reflects chemical weathering in the floodplains prior to deposition in the ocean, because these phases are less stable under conditions dominated by chemical weathering (Guidry & Mackenzie, 2000; White & Brantley, 1995).

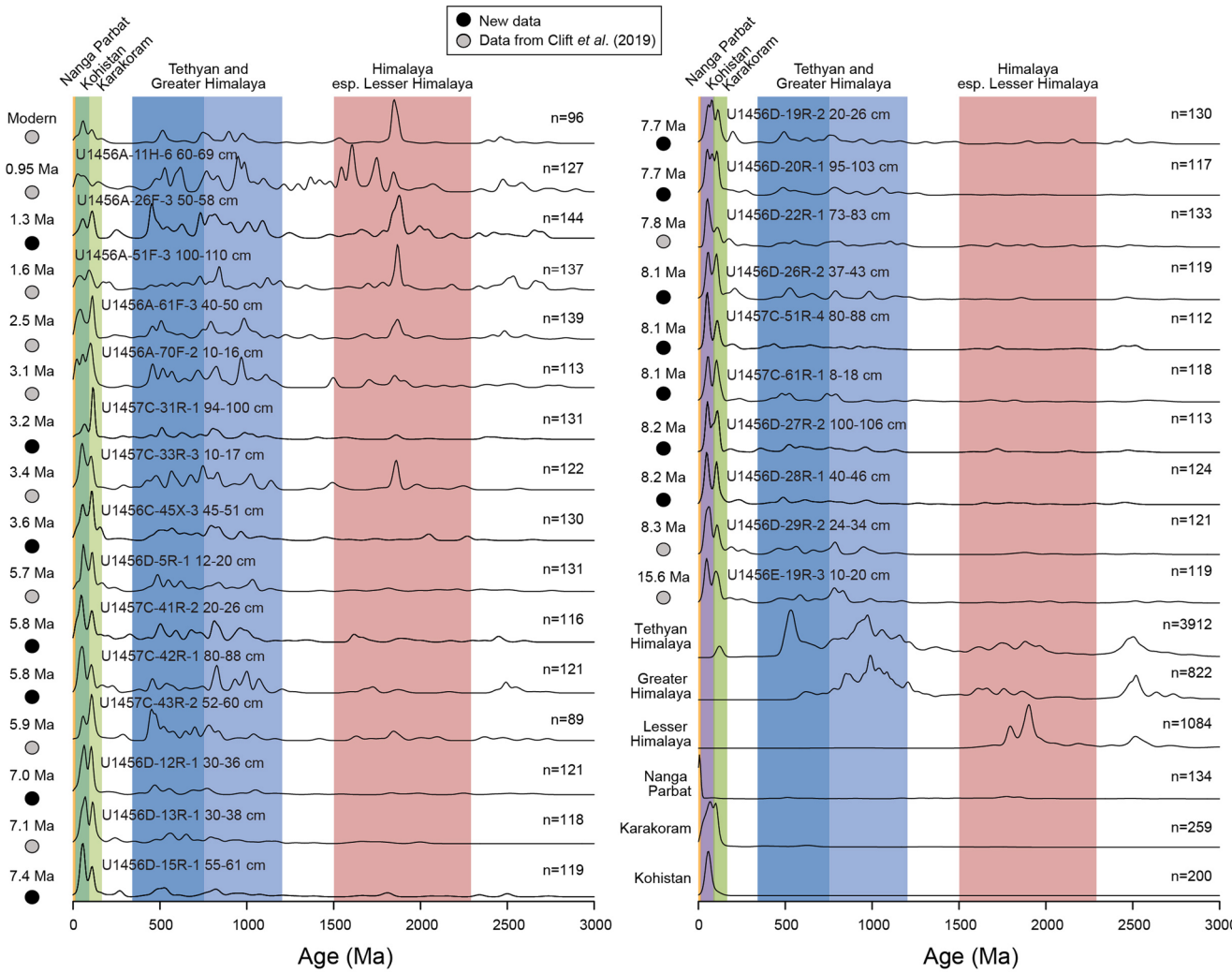

Figure 7. Kernal density estimate diagram showing the range of the zircon U-Pb ages for individual sand grains back to 3,000 Ma. Colored strips show the range of populations with diagnostic links to critical source terrains in the headwaters of the Indus. Data from the Siwaliks, as well as the Tethyan, Greater and Lesser Himalaya are compiled from DeCelles et al. (2004). Karakoram data is from is from Le Fort et al. (1983), Parrish and Tirrul (1989), Schärer et al. (1990), Fraser et al. (2001), and Ravikant et al. (2009). Nanga Parbat data is from Zeitler and Chamberlain (1991) and Zeitler et al. (1993). Transhimalayan data is from Honegger et al. (1982), Schärer et al. (1984), Krol et al. (1996), Weinberg and Dunlap (2000), Zeilinger et al. (2001), Dunlap and Wysoczanski (2002), Singh and France-Lanord (2002), and Ravikant et al. (2009). Samples are marked to show those published by Clift et al. (2019), and those presented new here.

However, all samples show this effect and there is a general consistency in the overall composition, so that we conclude that we are comparing sediments of a similar bulk character. All fan sediments show Zr abundances relatively close to the UCC average. There is a long-term temporal and stratigraphic decrease in Zr up-section, although the correlation is weak and is largely driven by an increase in low Zr samples after 10 Ma (Figure 6b).

6.2. Grain Size Effects

Before using the changing zircon U-Pb age spectra to infer changing sediment provenance, we explore the possible impact of grain size on controlling detrital zircon age spectra. Sediment grains are fractionated during transport because different densities and shapes affect their settling characteristics (Garzanti et al., 2009). Zircons all have the same density and roughly similar shape, but the size of the grains from a given source may vary and thus influence the final conclusions. If one source is associated with smaller or larger grains compared to other sources then this may prejudice the analysis, especially if the grains are too small (<30 microns) to be analyzed by the LA-ICP-MS U-Pb method. Certainly, grains smaller than those that can be dated are present in sediments,

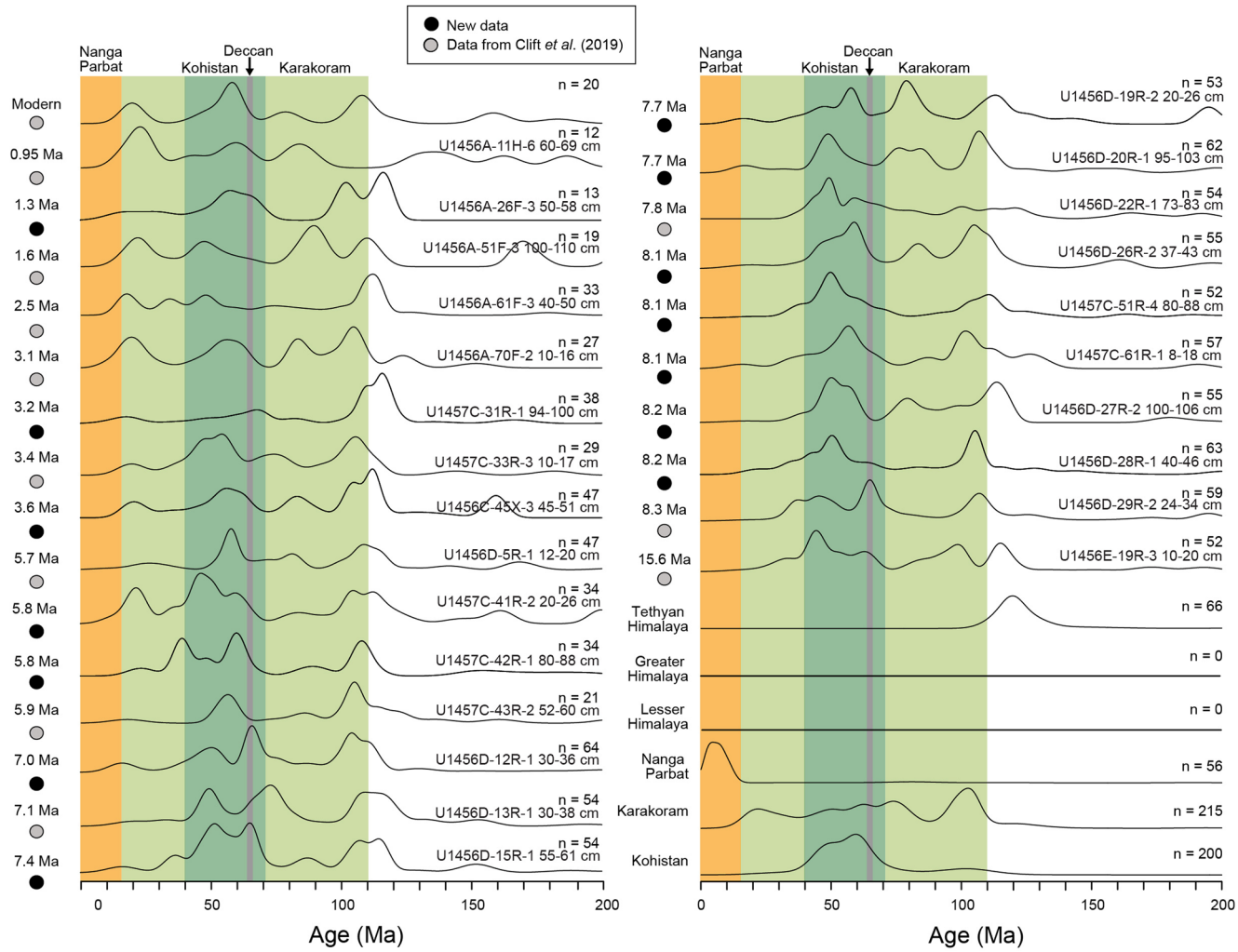

Figure 8. Kernal density estimate diagram showing the range of the zircon U-Pb ages for individual sand grains back to 200 Ma. Colored strips show the range of populations with diagnostic links to critical source terrains in the headwaters. See Figure 6 caption for data sources.

as seen by optical microscope and Raman spectroscopy methods (Andò et al., 2020) and this may introduce a bias to the age spectra and thus the interpretation. However, Garzanti et al. (2009) demonstrated that this effect was moderate in the Ganges-Brahmaputra catchment, which has strong similarities to the Indus. We plot major, provenance-related age populations (0–15, 40–70, 70–110, 300–750, 750–1,250, and 1,500–2,300 Ma) against median bulk grain size for all samples considered here to see if grain size plays a strong role in controlling the age spectra. Figure 10 shows that there is no strong correlation between sediment median grain size and the proportion of various provenance-sensitive age groups. However, we note that the four coarsest sediments (>100 μm) do contain more 750–1,250 and 1,500–2,300 Ma grains compared to the 40–70 and 70–110 Ma groups. The effect is especially strong with the 1,500–2,300 Ma group. In contrast to work on the Amazon River by Lawrence et al. (2011) who showed that older grains were significantly smaller than younger ones, the reverse may be true in the Indus. It is however noteworthy that the coarser sediments are all younger than 3.0 Ma and as demonstrated below the provenance inferred from similar aged finer sediment is not greatly different and also consistent with neighboring bulk sediment Nd isotope and heavy mineral constraints. We conclude that there may be a grain size issue with the coarsest sediment, but that this is not dominant in controlling the U-Pb age spectra.

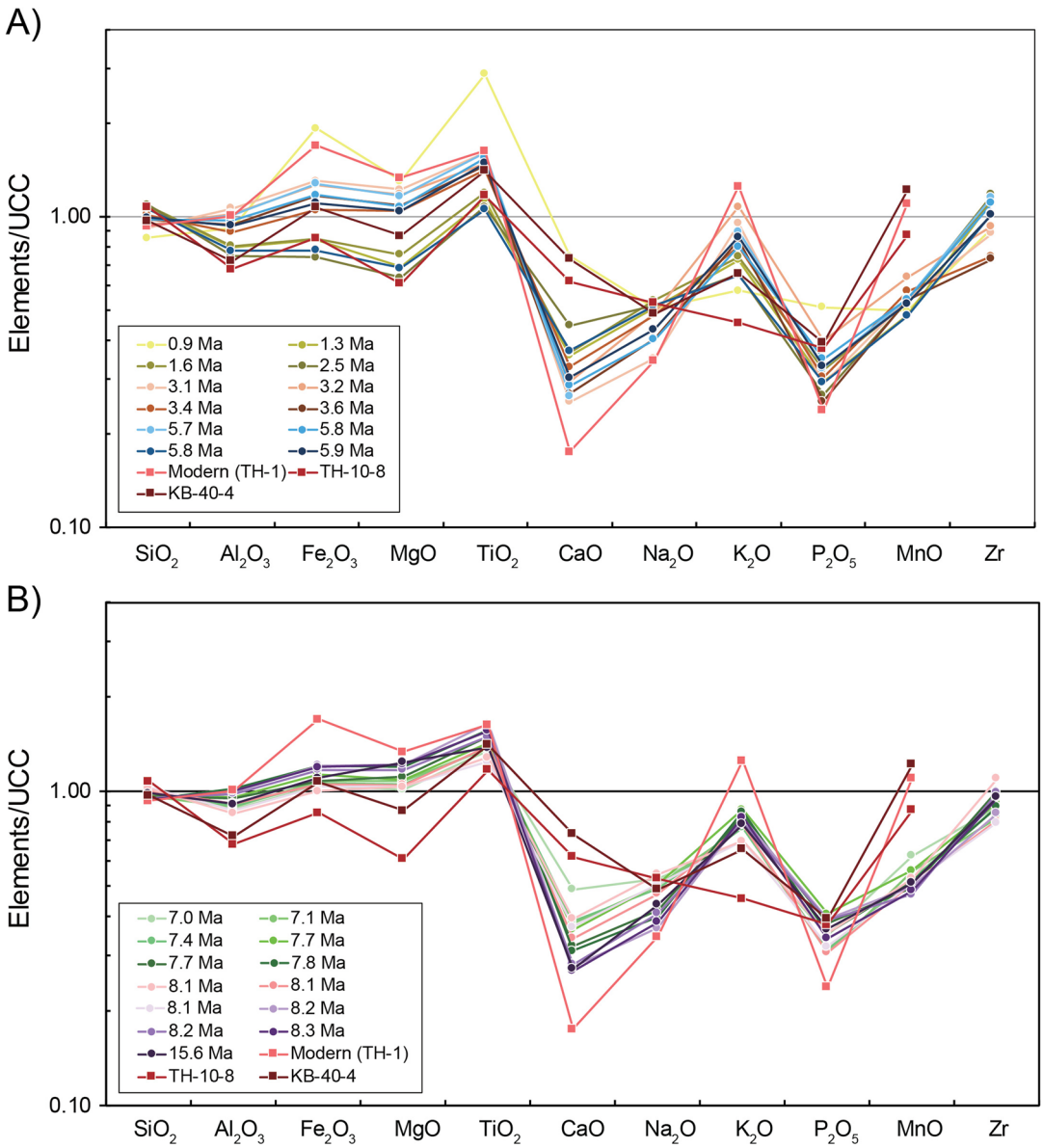

Figure 9. Upper continental crust normalized compositions of the sediments whose zircons are the focus of the study. Bulk settlement compositions are normalized according to the average of the continental crust from Taylor and McLennan (1995). Part A plots data from samples younger than 7 Ma and Part B shows data from samples 7 Ma and older.

6.3. U-Pb Zircon Ages

Zircon U-Pb age spectra are used to track the provenance evolution of sediment reaching the Arabian Sea by comparing them with bedrock zircon U-Pb age signatures of possible source areas (Figure 7). The abundance of grains younger than 200 Ma correlates well with young bedrocks from the Indus Suture Zone, particularly the Karakoram, as well as to a lesser extent Kohistan, the Transhimalaya and Nanga Parbat (Figure 8).

The abundance of these young zircon grains clearly points to sediment being supplied by the Indus River and not by peninsular India, where no magmatism <200 Ma is known outside the Deccan Plateau. Detrital zircon grains older than 350 Ma largely correlate with various bedrock sources known in the Himalaya. Detrital zircon age modes between 350 and 750 Ma have been correlated with bedrock sources in the Tethyan Himalaya (Alizai et al., 2011), although it is generally agreed that there is little real difference in terms of U-Pb ages between Tethyan and Greater Himalayan zircon signatures (Gehrels et al., 2011), and these are in any case not always mapped

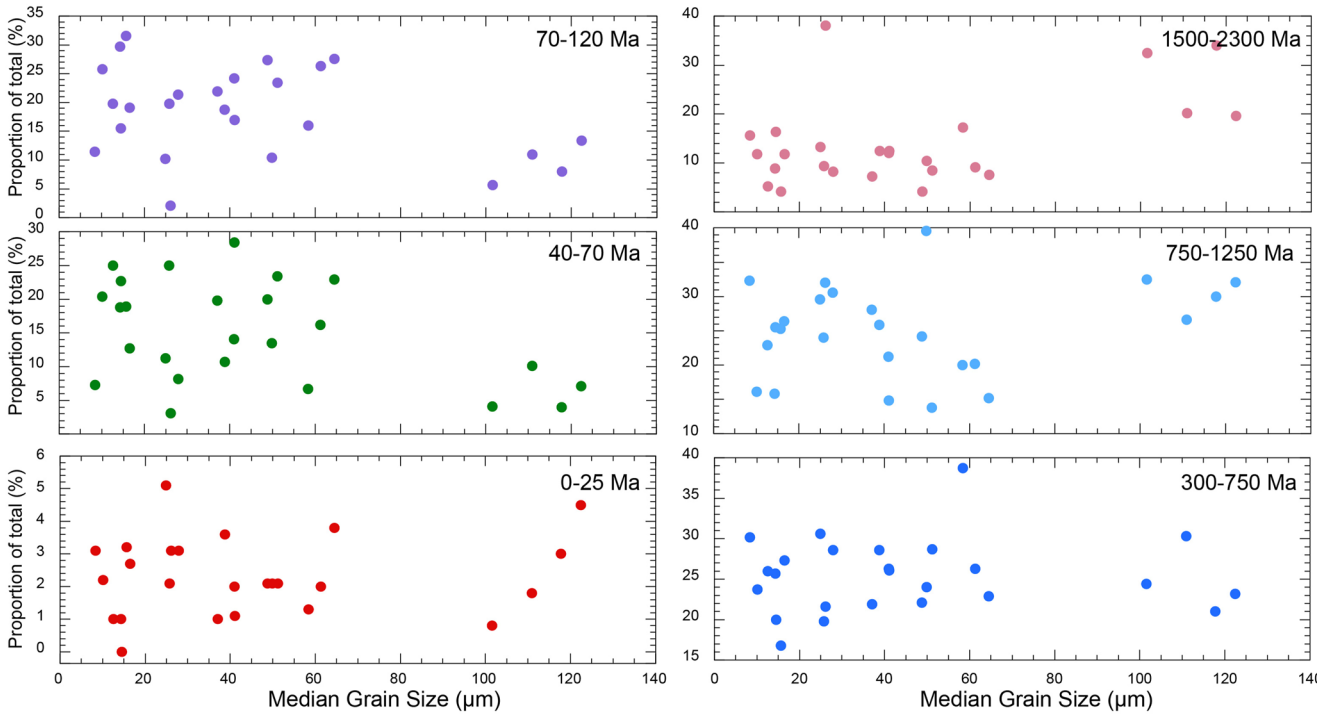

Figure 10. Plots of relative abundance of provenance sensitive zircon age populations in individual samples compared with sample median grain size. The coarsest samples show preference for the oldest U-Pb ages and a relative lack of the younger populations.

consistently by different groups (Webb, 2013). Consequently, zircons with ages between 350 and 1,250 Ma could be derived from either source. The older samples show relatively low abundance of grains in this age range, but these increased in frequency significantly starting at 5.9 Ma and become very abundant over the last few million years. Older grains, dating between 1,500 and 2,300 Ma, are particularly common in ILH sources, although they are also present in smaller amounts in the Tethyan and Greater Himalaya (DeCelles et al., 2000; Gehrels et al., 2011). These mainly Paleoproterozoic zircon grains are almost entirely absent from Miocene samples from the Laxmi Basin, but show a marked increase beginning at 5.9 Ma, and became very abundant beginning at 1.6 Ma (Figure 7). We therefore interpret these patterns to indicate a progressive increase in erosion from the Himalaya starting after 7.0 Ma, and especially starting at 5.9 Ma, with strong erosion from the Tethyan and Greater Himalaya.

The Greater and Lesser Himalayan material is largely provided by the Punjabi tributaries lying east of the Indus mainstream (Alizai et al., 2011). After 3.0 Ma there is a dramatic increase in erosional flux from the Lesser Himalaya, which have had a strong influence on the river system since the onset of the Holocene (Clift, Giosan, et al., 2008; Clift et al., 2004). This change could reflect an in increase in relative discharge from the Punjabi tributaries through time and/or a temporal change in the composition of these streams. Study of the foreland Siwalik sequences in the eastern part of the Indus catchment shows increasing erosion from the ILH starting in the Late Miocene (Najman et al., 2009).

If we only consider zircon grains younger than 200 Ma then we can see that there is evidence of erosion, from both Kohistan and from the Karakoram, in most of the samples analyzed (Figure 8). Kohistan is particularly noteworthy for having zircon dated between 40 and 70 Ma (Alizai et al., 2011; Zhuang et al., 2018), although there are similar aged units in the Karakoram as well. However, zircon grains older than 70 Ma but younger than 110 Ma, as well as dating 15–40 Ma are almost exclusively known only from Karakoram bedrock sources (Searle, 1996). The 3.2 Ma sample does not show the younger 40–70 Ma population, suggesting that it did not receive significant material from Kohistan/Ladakh. Although the relative contribution from Kohistan and the Karakoram changes on short time scales, the net Kohistan flux is quite small and changes in provenance on 10^5 year timescales are dominated by swings between the Himalaya and Karakoram, which have been linked in the recent geologic past

to fluctuations in the summer monsoon rainfall associated with glacial orbitally modulated cycles (Clift, Giosan, et al., 2008).

The youngest (<15 Ma) zircon grains are more enigmatic in terms of their provenance. While very young zircons are known from the present-day Nanga Parbat Massif, these are generally younger even than the 15 Ma zircon U-Pb age component observed in many of the samples (Zeitler et al., 1993). Our new data also show an increased influx from bedrock sources with very young (<15 Ma) zircon starting at 3.0 Ma, as well as a brief appearance at around 5.8 Ma. It is possible that this increase starting at 3.0 Ma reflects the emergence of Nanga Parbat, although we cannot exclude the influence of other young sources in the southern Karakoram metamorphic belt, which also contains rocks of this age and has experienced very rapid exhumation in the last few million years (Rolland et al., 2001; Wallis et al., 2016). Because the Deccan Plateau volcanic rocks were erupted rather quickly around 65 Ma, it is hard to completely exclude their influence because grains of a similar age are also known in Kohistan and in the Karakoram. However, the erosion from the Deccan Plateau would not account for the other young grains and an influx from that area should result in a clear peak age at 65 Ma, which is not observed.

We also assess the evolving provenance of sediments in Laxmi Basin using a multidimensional scalar (MDS) analysis of the detrital zircon U-Pb dates (Vermeesch et al., 2016). In this plot, which is a type of principle component analysis, samples with similar age spectra plot close to one another, while distinct samples are far separated. Figure 11a shows all the detrital data, along with modern river mouth and delta samples (KB-40) dating from shortly after the LGM (Clift, Giosan, et al., 2008). The MDS analysis shows clear and coherent patterns. Samples deposited at and after 1.6 Ma, are relatively similar to the modern river. In contrast, the oldest samples plot in a cluster suggesting a similar Miocene provenance and a subsequent progressive shift from right to left with decreasing depositional age, although with some reversals, most notably at 3.2 and 3.6 Ma. This reflects an overall shift in the zircon age spectra through time. Nonetheless, the LGM sample has stronger similarities with sediments deposited on the fan during the Late Miocene. Earlier work implied that erosion during the LGM was focused in the Karakoram (Clift, Giosan, et al., 2008) compared to the modern river or during the Holocene when the summer monsoon was strong (Caley et al., 2014; Fleitmann et al., 2003; Gupta et al., 2003). The new data indicate that older Miocene samples were also deriving their material from Karakoram sources, and this was followed by a shift to more Himalayan sources, especially in the last few million years. The plot implies that the change might be step wise, with a change starting between 7.0 and 5.9 Ma and accelerating again at 1.6 Ma.

The fact that the youngest turbidite sands are most similar to the modern interglacial river, and do not have the composition of the Indus shortly after the LGM, also implies that most of the sediment deposited in the Indus Fan has been eroded during interglacial times when the monsoon was strong, even if final deposition did not occur until the sea level fell during the onset of the subsequent glaciation. We envisage fast interglacial erosion generating great volumes of sediment, which is then mobilized, transported, and delivered to the delta as the rains strengthened (Jonell et al., 2017). The sediment would then be stored on the shelf or in the upper canyon during sea level high stands before being eroded and redeposited as sea level fell (Clift & Jonell, 2021; Li et al., 2018). This emphasizes the importance of monsoon intensity in controlling erosion and sediment delivery in the Western Himalaya.

We also compare the Arabian Sea sediments with known zircon ages from bedrock sources themselves. Figure 11b shows the progressive changes from the Miocene to the present and emphasizes the fact that the stratigraphically oldest detrital zircon samples plot closest to sources in the Karakoram and have similarities with analyses from the mainstream (upper reaches) of the Indus River, before it mixes with the Himalaya-draining Eastern tributaries, such as the Jhelum, Chenab, Ravi, Sutlej, and Beas (Figure 1). Conversely, the stratigraphically youngest sediments plot on this diagram closest to Himalayan sources and have greater similarity not only to the modern river mouth, but also with Himalayan tributaries such as the Ravi, Chenab, and Jhelum rivers.

These data also imply that Nanga Parbat has not been a very important contributor to the bulk sediment flux. Whether this is actually true or not is not entirely apparent because the bedrock analyses from Nanga Parbat were focused on igneous rocks in the center of that metamorphic massif and might not be representative of the net erosional flux from this particular source. However, the relationships displayed in Figure 11b can be readily explained as a simple mixing between Karakoram and Himalayan sources, with a progressive shift toward the Himalaya through time.

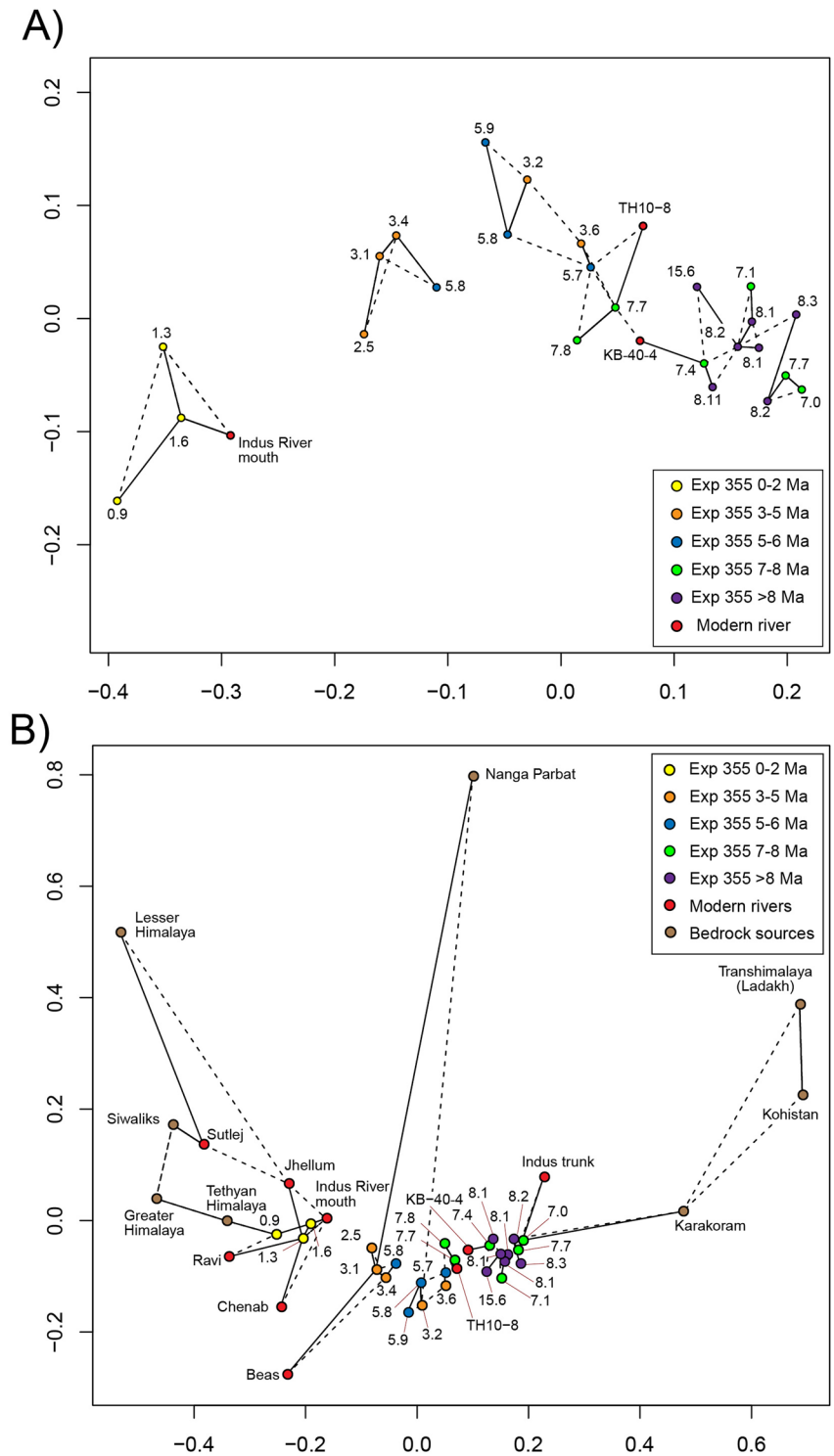

Figure 11. Multidimensional scalar diagrams made from zircon U-Pb age data showing (a) how the different sediment samples from International Ocean Discovery Program Expedition 355 compare with one another and post-glacial sediments from the Indus delta (TH-10-8 and KB-40-4) and (b) with the major source terranes in the Indus catchment, as well as the modern rivers of the Indus catchment, that is, the main or trunk stream of the Indus, upstream of Attock, and its major eastern tributaries. Solid lines join sediments to their most similar neighbor, while dashed lines join the next most similar. Sources of bedrock age data come from the literature, as described in Figure 6. River data is from Alizai et al. (2011). Note that sediments older than 5 Ma plot toward the right in Figure 10b, in the direction of Karakoram bedrock sources, whereas there is a progressive migration toward the left, toward Himalayan sources after that time. Diagram was constructed using the statistical package of Vermeesch et al. (2016).

6.4. Unmixing Sources

To further characterize the evolving source of sediment to the Indus Fan we employ the unmixing software of Sundell and Saylor (2017), which analyzes the U-Pb age spectra from each of the samples and compares them with the defined end-member compositions of the different source ranges compiled from the published literature. This approach is particularly suitable for application in the Western Himalaya where the U-Pb source signatures are well defined and often unique. Data from the Tethyan, Greater and Lesser Himalaya were compiled from DeCelles et al. (2004). Data from the Karakoram are from Le Fort et al. (1983), Parrish and Tirrul (1989), Schärer et al. (1990), Fraser et al. (2001), and Ravikant et al. (2009). Data from Nanga Parbat are from Zeitler and Chamberlain (1991) and Zeitler et al. (1993). Data from the Transhimalaya are from Honegger et al. (1982), Schärer et al. (1984), Krol et al. (1996), Weinberg and Dunlap (2000), Zeilinger et al. (2001), Dunlap and Wysoczanski (2002), Singh et al. (2007), and Ravikant et al. (2009).

This unmixing method uses a Monte Carlo approach to estimate the contributions from the different defined sources to generate the modes and modal abundances of U-Pb ages seen in the sediment samples. Because this is relatively objective the method is considered robust for analyzing potential source contributions, assuming that the sources themselves have been well characterized. The bedrock sources of the Indus catchment have significant differences between them and are some of the best characterized worldwide. Results from the Monte Carlo simulations are provided in Table S3, showing the output using all three statistical comparison methods, that is, cross-correlation, the V value in the Kuiper test as well as the D value in the K-S test. The method involves creating 10,000 model mixed sediments using the defined bedrock source end members. The DZMix software then compares the model with the measured spectra and retains the best 1% of these models to estimate which sources were contributing the sampled material. We favor the unmixing models derived from the cross-correlation approach as being geological reasonable and favored by Sundell and Saylor (2017).

The results of our unmixing calculations show a progressive long-term provenance evolution that is consistent with that seen in the MDS diagram (Figures 11 and 12). The very oldest sample deposited at 15.6 Ma shows a dominance of sediment derived from the Karakoram (58 ± 12%) and from the Tethyan and Greater Himalaya (34 ± 11%). Most of the Miocene samples dated between 8.3 and 7.0 Ma are more dominated by material from the Karakoram (average 70 ± 15%) but also usually show significant Tethyan and Greater Himalayan contributions (average 24 ± 13%). This Himalayan component is particularly noteworthy at 8.1 Ma (26%), 7.8 Ma (28%), and 7.4 Ma (36%) during this interval. The proportion of Karakoram zircons shows a significant decrease starting no later than 5.9 Ma and again at 3.1 Ma. The average contribution from these ranges fell from 70% at 8.3–7.0 Ma to 35% between 5.9 and 5.7 Ma but was similar at 34 ± 12% during 3.6–2.5 Ma. Average flux from the Karakoram fell again during 1.6–0.95 Ma when the contribution averaged just 7 ± 5%.

Our study provides new data for a plethora of samples for the period 8.3–7.0 Ma when the Karakoram is on average the largest single source. However, the variability of this flux ranges from 51% to 84% of the total, which is nonetheless lower than the 55%–21% variation seen since the LGM at 20 ka. Short-term variations in erosion are known to be caused by climatic variations (Clift, Giosan, et al., 2008) and are unlikely to be limited to the onset of Northern Hemisphere Glaciation (NHG), especially as the 8.3–7.0 Ma period is known to be one of climatic transition (Clift et al., 2020), marked by a sharp drop in C3 vegetation compared to C4 (Feakins et al., 2020; Suzuki et al., 2020). Since the onset of NHG storage of sediment in the lower reaches of the river and on the continental shelf acts to buffer sediment supply to the deep-sea fan and causes large scale homogenization of the erosional signal to the submarine fan across complete sea-level cycles (Clift & Jonell, 2021). This effect would be less when sea-level variability was reduced, so that changes in provenance on times scales of a few 10^5 year likely reflect true variations in erosion pattern that are most readily attributed to changes in monsoon rainfall intensity rather than slower acting tectonic forcing.

From 3.6 Ma onwards the Himalaya dominated as sources to the submarine fan, with significant amounts of material from the ILH first appearing at 1.6 Ma. Average flux from the Greater and Tethyan Himalaya was 55 ± 12% at 3.6–2.5 Ma but just 5 ± 5% from the ILH. These values reached 72 ± 8% and 17 ± 6% respectively at 1.6–0.95 Ma. The sample dated as having been deposited at 0.95 Ma is anomalous for being very similar in source signature to Tethyan and Greater Himalayan bedrocks source (91 ± 5%). However, we note that fission track data indicate that this sample was derived from peninsular India (Zhou et al., 2019) and so it is not considered further in our reconstruction of Himalayan erosion.

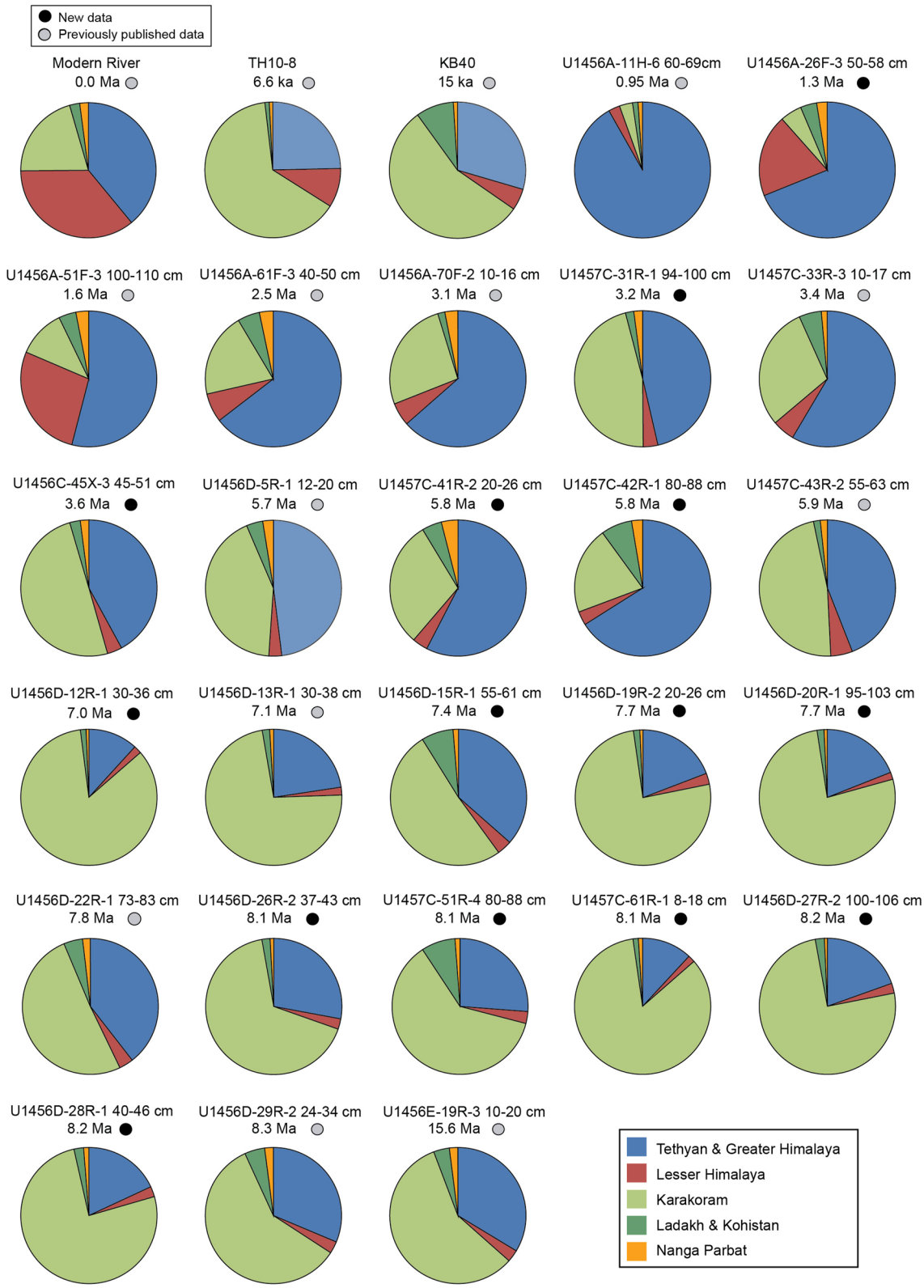

Figure 12. Pie diagrams showing the predicted source compositions of the zircon populations in sands from the Laxmi Basin as unmixed using the software of Sundell and Saylor (2017). Note the significant reduction in flux from the Karakoram starting ~5.7 and again at 3.0 Ma. Samples are marked to show those published by Clift et al. (2019), and those presented new here.

The unmixing analysis largely mirrors the pattern shown by the MDS diagram, in showing a long-term increase in erosion from the Himalaya relative to the Karakoram, although short-term variations are seen and the discontinuous character of the record makes the precise timing of some of the more dramatic changes hard to pinpoint. All of the samples contain a small amount of very young <15 Ma zircons. None of the samples analyzed show a close similarity with post-LGM river compositions. Delta samples deposited at 6.6 and 15 ka are strongly enriched in Karakoram-derived grains (52% and 55%) compared to fan sediments deposited at and after 1.6 Ma (3%–11%). This short term variability is interpreted to reflect the rapid changes in erosion patterns linked to monsoon strength, modulated by glacial cycles since the onset of the NHG (Clift, Giosan, et al., 2008).

6.5. Relationships to Climate Change and Tectonics

The increase in the relative flux from the Himalaya since the Middle Miocene represents the progressive unroofing of these units. Structural reconstructions of the Western Himalaya predict that prior to 5.4 Ma the Greater and Lesser Himalaya were not exposed (Webb, 2013) implying that the Himalayan contribution was derived entirely from the Tethyan Himalaya during the Miocene. This prediction is at odds with mica Ar-Ar and Nd isotope studies of the Siwalik Group from the eastern Indus Catchment that indicates at least some Greater Himalayan exposure since the Early Miocene (White et al., 2002). Nonetheless, the first major flux of Himalayan zircons to the Indus submarine fan is dated at 8.0–7.8 Ma, although widespread Himalayan unroofing may not have started until 5.9 Ma, followed by ILH unroofing starting around 1.6 Ma. As we are not able to distinguish between Tethyan and Greater Himalaya derived sediment we focused on the first appearance of significant amounts of 1,500–2,300 Ma, ILH detritus.

The timing of Lesser Himalayan unroofing may reflect the development of the thrust duplex, which characterizes the structure of the Lesser Himalaya in this area (Huyghe et al., 2001; Webb, 2013). Previous studies considered these ranges to have been exposed somewhat before 1.6 Ma. Colleps et al. (2019) argue for Lesser Himalayan exhumation starting after 16 Ma, although Meigs et al. (1995) favored exhumation starting after 11 Ma, as motion on the MBT commenced. Integrated metamorphic and geochronologic data indicate rapid cooling of the ILH before 6 Ma, following peak metamorphism around 10 Ma (Caddick et al., 2007; Thiede et al., 2009). Further east in Nepal duplexing of the ILH is proposed to have only started in the Pliocene (Robinson et al., 2006).

Exhumation should not however be confused with unroofing and erosion. Rapid cooling does not require synchronous unroofing. Thermochronometric measurements of the source rocks constrain the exhumation of source bedrocks over long periods of time, which contrasts with the provenance signal in a single turbidite sand bed, which reflects erosion over shorter periods of time, ~100 ky in the last 900 ka, representing a glacial cycle. As such the erosion patterns recorded in the provenance of a sedimentary bed are more susceptible to rapid changes in erosion caused by climate change, and not just the tectonically driven exhumation derived from bedrock studies. Even before the onset of the NHG climate is susceptible to various relatively rapid forcing processes, including orbital cycles. Study of the Siwalik Group in the area of the Beas River Valley on the eastern edge of the Indus catchment indicated an initial exposure of these units around 9 Ma and significant exposure by 6 Ma based on Nd isotope data (Najman et al., 2009). Colleps et al. (2019) preferred a date for this initial exposure at 3–7 Ma in NW India, while favoring an older age of 9–11 Ma in Nepal. These ages all postdate the major flux of ILH material noted in the Laxmi Basin.

Our new data support the findings of Clift et al. (2019) that the exposure of Himalayan units in Western India may only reflect the local situation in the paleo-Beas River area, but that widespread regional exposure of the ILH units comes somewhat later. While Clift et al. (2019) favored increased ILH erosion starting at 1.9 Ma our new zircon data imply that 1.6 Ma is a more accurate age for this this transition. Our result contrasts with the suggestion by Myrow et al. (2015) that the ILH were widely exposed and eroding by 16 Ma across much of the Himalayan front. Although we cannot exclude this from happening further east in the Ganges Basin our data do not support this over a wide area of the Western Himalaya until much later.

Uplift of the ILH Duplex would have created a topographic barrier, susceptible to erosion by monsoon rains that were focused along this topographic front. The increasingly Himalayan character of the total zircon input comes at a time when the summer monsoon rains were generally weakening after ~8 Ma (Dettman et al., 2001), or after 7.7 Ma based on new environmental data from Site U1456 (Clift et al., 2020) (Figure 13). Moisture delivery to this area from the winter westerlies has also been shown to have reduced around 7 Ma (Vögeli et al., 2017). In

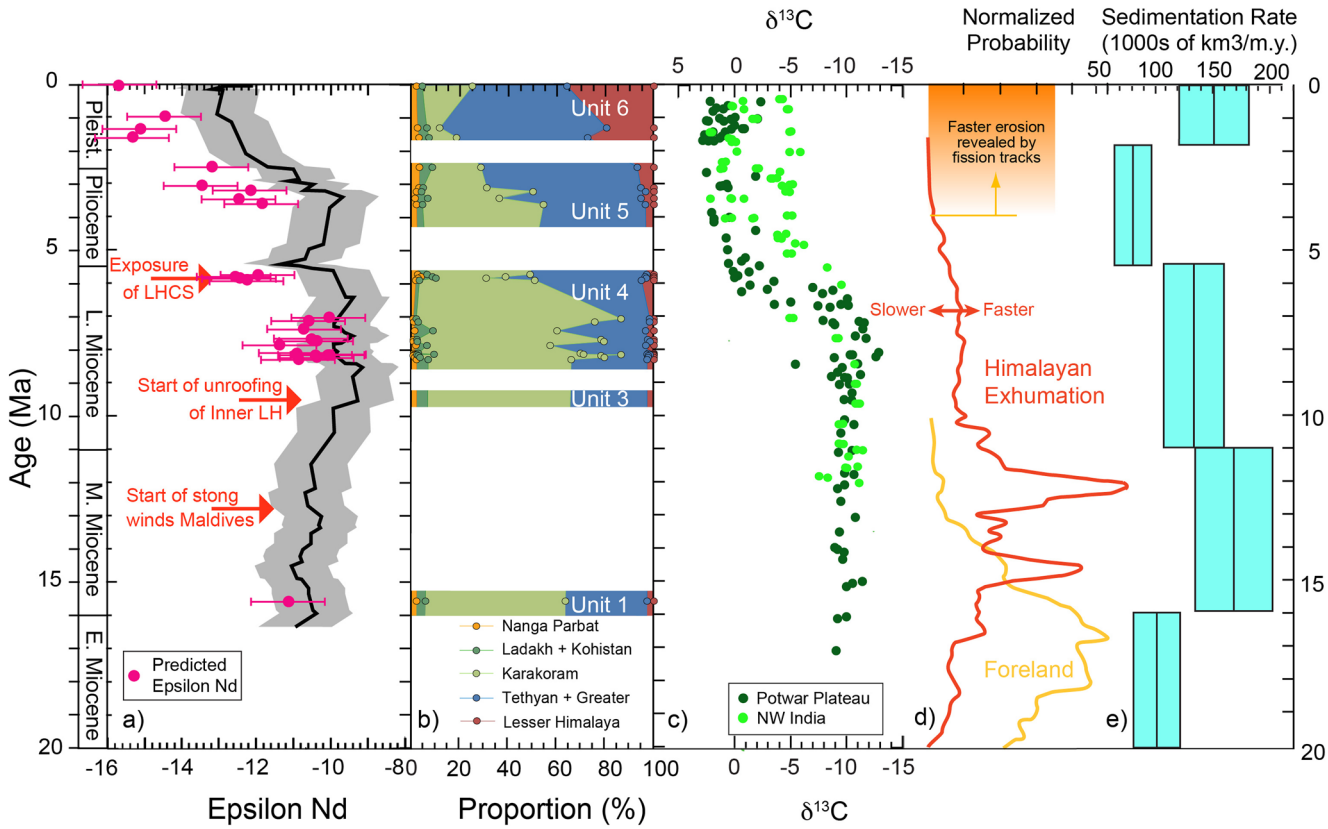

Figure 13. Comparison of climate, erosion, and exhumation proxies in the Himalaya. (a) Smoothed Nd isotopic history for the Indus River with gray background showing effective uncertainties from Clift et al. (2018). (b) Breakdown of the sources of detrital zircons based on the unmixing procedure of Sundell and Saylor (2017) but excluding the 0.95 Ma sample, which was derived from peninsular India. Units follow the scheme of Routledge et al. (2020). (c) Carbon isotope character of pedogenic carbonate in Pakistan as an indicator of dominant vegetation in the Potwar Plateau of Pakistan (Quade et al., 1989), and NW India (Singh et al., 2011). (d) Relative exhumation rates of the Greater Himalaya tracked by bedrock Ar-Ar dating (Clift, Hodges, et al., 2008) and zircon fission track from foreland basin sediment (Chirouze et al., 2015). (e) Rates of sediment supply to the Arabian Sea calculated from regional seismic (Clift, 2006).

the recent geologic past, since the LGM, strong Himalayan rather than Karakoram erosion has occurred when the summer monsoon was strong, during interglacial times and not when it was weak during glacial times (Clift, Giosan, et al., 2008). The increase in Himalayan erosion over longer periods of time, correlating with the weakening monsoon, is the opposite of this shorter-term trend. It is possible that solid Earth tectonic forces, rather than climate, have dominated the long-term evolution of erosion, although the temporal correlation of provenance and aridity is suggestive of some climatic control.

All of the samples show the presence of very young zircons (<15 Ma) that possibly correlate with bedrock dates from Nanga Parbat, although these are never very numerous. It is also possible that some of these young ages may in fact be derived from erosion of fast exhuming rocks in parts of the southern Karakoram (Wallis et al., 2014). However, even if that this material was derived from Nanga Parbat, the low abundance of such zircon grains in Laxmi Basin sediments would suggest that this massif has not been generating very high proportions of sediment in the mainstream Indus river, unlike the situation in the eastern syntaxis (Garzanti et al., 2004; Stewart et al., 2008). This is consistent with the U-Pb zircon ages in the modern Indus River downstream of Nanga Parbat (Alizai et al., 2011) that show neither many <15 Ma zircons or older 1,500–2,300 Ma grains that would be associated with less deeply buried rocks but with the Lesser Himalayan affiliation typically made with Nanga Parbat (Whittington et al., 1999).

6.6. Comparing Nd Isotopes and Zircons

We compare our detrital zircon budget with that of the Nd budget published by Clift et al. (2019). Translating zircon budgets into rock erosion budgets is non-trivial due to bedrock zircon fertility variations. However,

whole-rock geochemical analysis of Alizai et al. (2012) suggested that on average the eastern, Himalaya-draining tributaries are around 2.2 times more fertile in zircon than the trunk Indus. If we simply use the source percentages from the zircon unmixing calculation described above and the average ε_{Nd} values for these different units then it is possible to predict the average composition of the bulk sediment through time. This is necessarily a simple, first-order comparison to establish whether the two methods indicate similar trends and ignores the fact that the Nd method is biased toward finer grained suspended sediments, while the zircon is more skewed toward coarser bed-load sediments. We use an ε_{Nd} value of −14.6 for the Greater and Tethyan Himalaya, −21.7 for the ILH, −9.3 for the Karakoram, −20 for Nanga Parbat, and +5.1 for Kohistan and the Transhimalaya based on synthesis of the bedrock data, but especially the composition of river sediments that are derived from wide areas of these ranges (Clift, Lee, et al., 2002). Transhimalaya Nd data are from Rolland et al. (2002), Singh and France-Lanord (2002), and Khan et al. (1997). Greater and Lesser Himalayan data are from Ahmad et al. (2000), Deniel et al. (1987), Inger and Harris (1993), and Parrish and Hodges (1996). Karakoram data are from Crawford and Searle (1992) and Schärer et al. (1990). In all cases, we use the ±1 ε_{Nd} point estimated for mixed sediment in the Indus River derived from repeat analyses of post-glacial Indus sediment (Jonell et al., 2018).

The results of this estimate are shown next to the smoothed long-term Nd isotope evolution from bulk sediment analysis (Clift et al., 2019) (Figure 13). We note that before 6 Ma the estimates overlap with the bulk sediment record that was derived from muddy lithologies, suggesting similar sources. After this time both the estimated and measured ε_{Nd} values became more negative. However, the predicted Nd isotope compositions are always more negative than those measured from the bulk sediment and this implies an overestimation in the flux from isotopically negative sources, that is, the Himalaya, using the zircon method. This is consistent with the geochemical data indicating that the Himalaya are more abundant in zircon than the Karakoram, but have similar concentrations of Nd (Alizai et al., 2011). As a result, our zircon budget (Figure 13) represents an overestimate of the influence of the Himalaya compared the Karakoram through time in terms of total rock eroded. Nonetheless, the overall trends in the two data sets are consistent and the reconstruction of increasing Himalayan erosion since 5.9 Ma may be considered robust. The correspondence of the Nd and zircon provenance records moreover affirms that the common, young (<120 Ma) zircon grains must be dominantly Karakoram-derived and not from Nanga Parbat because the latter is very negative in ε_{Nd} values, −20 compared to the more positive Karakoram (−9.3).

7. Conclusions

Sandy and silty sediments recovered from the Laxmi Basin in the Eastern Arabian Sea provide a long-term, albeit discontinuous erosional record derived from the Indus River and spanning the last 15.6 m.y. In this study, samples were taken from IODP Sites U1456 and U1457 for geochemical and geochronological analyses. Detrital zircon grains were dated by U-Pb methods to determine their provenance. The sediments themselves are defined as wackes and are relatively immature in composition, with bulk sediment characters, similar to those found in the Quaternary delta of the Indus and in its submarine canyon. They are readily distinguishable from sediments on the Western Indian Shelf, confirming their derivation from the Indus River and not the peninsula with one exception at 0.9 Ma. The sediments are mostly of silty sand to silt size, with only a few being classified as fine sand. Although the sediments are relatively depleted in Ca, Na and P relative to the UCC this reflects chemical weathering during transport and does not affect the provenance analysis conducted here.

Detrital zircon U-Pb ages fall into a number of categories which can be correlated with bedrock sources in the Himalaya. The ubiquitous presence of zircon grains younger than 200 Ma requires the sediments to be the erosional products of the Himalaya/Karakoram and not peninsular India. The progressive increase in zircon grains dating at 350–1,250 Ma, as well as 1,500–2,300 Ma, indicates that the erosional flux from the Himalaya increased through the studied time interval. Almost all the samples contain grains that could be derived from the Karakoram (or from Kohistan), and there is an appearance of very young zircon grains, younger than 15 Ma, that is especially marked since 3.2 Ma. Such young zircon grains may be from Nanga Parbat or parts of the eastern Karakoram.

Statistical analysis shows that there are a number of groupings and an increase in Himalayan erosion through time. High flux from the Himalaya was noted at 8.0–7.8 Ma and starting between 7.0 and 5.9 Ma. Since 1.6 Ma the sediments have been similar to the modern Indus River, but not like the glacial-era river, which has more similarities with the Miocene Laxmi Basin samples and with enhanced erosion in the Karakoram. Detrital zircon population unmixing techniques allow us to objectively confirm the progressive increase of Himalayan erosion

relative to the Karakoram from 24% Tethyan/Greater Himalaya at 7.0–8.3 Ma to 54%–55% at 2.5–5.9 Ma, and finally 72% after 1.6 Ma. There was also sharp rise in erosion from the ILH from 5% to 17% starting at 1.6 Ma. This is somewhat younger than the anticipated unroofing of these ranges derived from earlier foreland studies, although much of the earlier data comes from further east in the Ganges catchment. The shift to more Himalayan erosion through time occurs as the monsoon climate weakened, as well as when the ILD Duplex formed. This suggests that the changing patterns of erosion could be largely a function of solid Earth tectonic forces building topography, although the correlation of unroofing to the Late Miocene drying trend does raise the possible role for climate too, albeit in the opposite fashion to that seen since the LGM, when more Himalayan erosion correlates with strong summer monsoon rains.

Data Availability Statement

Data related to this study are available as tables within the article and from Mendeley (data.mendeley.com) at https://doi.org/10.17632/b57z79m4kj.1

Acknowledgments
This study was made possible by samples provided by the International Ocean Discovery Program. This work was partially funded by a grant from the USSSP, as well as additional funding from the Charles T. McCord Chair in petroleum geology at LSU, and the Chevron (Gulf) Centennial professorship and the UTChron Laboratory at the University of Texas. The authors also would like to acknowledge Lisa Stockli for assistance with zircon U-Pb data acquisition and reduction. This paper was improved thank to comments from two anonymous reviewers and Associate Editor Peter van der Beek.

References

Ahmad, T., Harris, N., Bickle, M., Chapman, H., Bunbury, J., & Prince, C. (2000). Isotopic constraints on the structural relationships between the Lesser Himalayan Series and the High Himalayan Crystalline Series, Garhwal Himalaya. *The Geological Society of America Bulletin*, *112*(3), 467–477. https://doi.org/10.1130/0016-7606(2000)112<467:icotsr>2.0.co;2

Alizai, A., Carter, A., Clift, P. D., VanLaningham, S., Williams, J. C., & Kumar, R. (2011). Sediment provenance, reworking and transport processes in the Indus River by U-Pb dating of detrital zircon grains. *Global and Planetary Change*, *76*, 33–55. https://doi.org/10.1016/j.gloplacha.2010.11.008

Alizai, A., Hillier, S., Clift, P. D., & Giosan, L. (2012). Clay mineral variations in Holocene terrestrial sediments from the Indus Basin; a response to SW Asian Monsoon variability. *Quaternary Research*, *77*(3), 368–381. https://doi.org/10.1016/j.yqres.2012.01.008

Amidon, W. H., Burbank, D. W., & Gehrels, G. E. (2005). U-Pb zircon ages as a sediment mixing tracer in the Nepal Himalaya. *Earth and Planetary Science Letters*, *235*(1–2), 244–260. https://doi.org/10.1016/j.epsl.2005.03.019

Andò, S., Aharonovich, S., Hahn, A., George, S. C., Clift, P. D., & Garzanti, E. (2020). Integrating heavy-mineral, geochemical and biomarker analyses of Plio-Pleistocene sandy and silty turbidites: A novel approach for provenance studies (Indus Fan, IODP Expedition 355). *Geological Magazine*, *157*(6), 929–938. https://doi.org/10.1017/S0016756819000773

Baral, U., Lin, D., & Chamlagain, D. (2015). Detrital zircon U-Pb geochronology of the Siwalik Group of the Nepal Himalaya: Implications for provenance analysis. *International Journal of Earth Sciences*, 1–19. https://doi.org/10.1007/s00531-015-1198-7

Bernet, M., van der Beek, P., Pik, R., Huyghe, P., Mugnier, J.-L., Labrin, E., et al. (2006). Miocene to recent exhumation of the central Himalaya determined from combined detrital zircon fission-track and U/Pb analysis of Siwalik sediments, western Nepal. *Basin Research*, *18*, 393–412. https://doi.org/10.1111/j.1365-2117.2006.00303.x

Bhattacharya, G. C. B., Chaubey, A. K., Murty, G. P. S., Srinivas, S., Sarma, K. V., Subrahmanyam, V., et al. (1994). Evidence for seafloor spreading in the Laxmi Basin, northeastern Indian Ocean. *Earth and Planetary Science Letters*, *125*, 211–220. https://doi.org/10.1016/0012-821x(94)90216-x

Bollinger, L., Avouac, J. P., Beyssac, O., Catlos, E. J., Harrison, T. M., Grove, M., et al. (2004). Thermal structure and exhumation history of the Lesser Himalaya in central Nepal. *Tectonics*, *23*(5), 19. https://doi.org/10.1029/2003TC001564

Bookhagen, B., Thiede, R. C., & Strecker, M. R. (2005). Late Quaternary intensified monsoon phases control landscape evolution in the northwest Himalaya. *Geology*, *33*(2), 149–152. https://doi.org/10.1130/G20982.1

Burbank, D. W., Blythe, A. E., Putkonen, J., Pratt-Sitaula, B., Gabet, E., Oskins, M., et al. (2003). Decoupling of erosion and precipitation in the Himalayas. *Nature*, *426*, 652–655. https://doi.org/10.1038/nature02187

Caddick, M. J., Bickle, M. J., Harris, N. B. W., Holland, T. J. B., Horstwood, M. S. A., Parrish, R. R., et al. (2007). Burial and exhumation history of a Lesser Himalayan schist: Recording the formation of an inverted metamorphic sequence in NW India. *Earth and Planetary Science Letters*, *264*(3–4), 375–390. https://doi.org/10.1016/j.epsl.2007.09.011

Caley, T., Roche, D. M., & Renssen, H. (2014). Orbital Asian summer monsoon dynamics revealed using an isotope-enabled global climate model. *Nature Communications*, *5*, 5371. https://doi.org/10.1038/ncomms6371

Calvès, G., Huuse, M., Clift, P. D., & Brusset, S. (2015). Giant fossil mass wasting off the coast of West India: The Nataraja submarine slide. *Earth and Planetary Science Letters*, *432*, 265–272. https://doi.org/10.1016/j.epsl.2015.10.022

Catlos, E. J., Harrison, T. M., Kohn, M. J., Grove, M., Ryerson, F. J., Manning, C. E., et al. (2001). Geochronologic and thermobarometric constraints on the evolution of the Main Central Thrust, central Nepal Himalaya. *Journal of Geophysical Research*, *106*(B8), 16177–116204. https://doi.org/10.1029/2000jb900375

Chirouze, F., Huyghe, P., Chauvel, C., van der Beek, P., Bernet, M., & Mugnier, J.-L. (2015). Stable drainage pattern and variable exhumation in the western Himalaya since the Middle Miocene. *The Journal of Geology*, *123*, 1–20. https://doi.org/10.1086/679305

Clift, P., Gaedicke, C., Edwards, R., Lee, J., II, Hildebrand, P., Amjad, S., et al. (2002). The stratigraphic evolution of the Indus Fan and the history of sedimentation in the Arabian Sea. *Marine Geophysical Researches*, *23*(3), 223–245.

Clift, P. D. (2006). Controls on the erosion of Cenozoic Asia and the flux of clastic sediment to the ocean. *Earth and Planetary Science Letters*, *241*(3–4), 571–580. https://doi.org/10.1016/j.epsl.2005.11.028

Clift, P. D., & Blusztajn, J. S. (2005). Reorganization of the western Himalayan river system after five million years ago. *Nature*, *438*(7070), 1001–1003. https://doi.org/10.1038/nature04379

Clift, P. D., Campbell, I. H., Pringle, M. S., Carter, A., Zhang, X., Hodges, K. V., et al. (2004). Thermochronology of the modern Indus River bedload New insight into the control on the marine stratigraphic record. *Tectonics*, *23*(TC5013). https://doi.org/10.1029/2003TC001559

Clift, P. D., Giosan, L., Blusztajn, J., Campbell, I. H., Allen, C. M., Pringle, M., et al. (2008). Holocene erosion of the Lesser Himalaya triggered by intensified summer monsoon. *Geology*, *36*(1), 79–82. https://doi.org/10.1130/G24315A.1

Clift, P. D., Giosan, L., Carter, A., Garzanti, E., Galy, V., Tabrez, A. R., et al. (2010). Monsoon control over erosion patterns in the western Himalaya: Possible feed-backs into the tectonic evolution. In P. D. Clift, R. Tada, & H. Zheng (Eds.), *Monsoon evolution and tectonic-climate linkage in Asia* (pp. 181–213). Geological Society.

Clift, P. D., Hodges, K., Heslop, D., Hannigan, R., Hoang, L. V., & Calves, G. (2008). Greater Himalayan exhumation triggered by Early Miocene monsoon intensification. *Nature Geoscience*, *1*, 875–880. https://doi.org/10.1038/ngeo351

Clift, P. D., & Jonell, T. N. (2021). Monsoon controls on sediment generation and transport: Mass budget and provenance constraints from the Indus River catchment, delta and submarine fan over tectonic and multi-millennial timescales. *Earth-Science Reviews*, 103682. https://doi.org/10.1016/j.earscirev.2021.103682

Clift, P. D., Kulhanek, D. K., Zhou, P., Bowen, M. G., Vincent, S. M., Lyle, M., et al. (2020). Chemical weathering and erosion responses to changing monsoon climate in the Late Miocene of Southwest Asia. *Geological Magazine*, *157*(6), 939–955. https://doi.org/10.1017/S0016756819000608

Clift, P. D., Lee, J. I., Hildebrand, P., Shimizu, N., Layne, G. D., Blusztajn, J., et al. (2002). Nd and Pb isotope variability in the Indus River system; implications for sediment provenance and crustal heterogeneity in the western Himalaya. *Earth and Planetary Science Letters*, *200*(1–2), 91–106. https://doi.org/10.1016/S0012-821X(02)00620-9

Clift, P. D., Shimizu, N., Layne, G., Gaedicke, C., Schlüter, H. U., Clark, M. K., et al. (2001). Development of the Indus Fan and its significance for the erosional history of the western Himalaya and Karakoram. *The Geological Society of America Bulletin*, *113*, 1039–1051. https://doi.org/10.1130/0016-7606(2001)113<1039:dotifa>2.0.co;2

Clift, P. D., Zhou, P., Stockli, D. F., & Blusztajn, J. (2018). Regional Pliocene exhumation of the Lesser Himalaya in the Indus drainage. *Solid Earth*. https://doi.org/10.5194/se-2018-132

Clift, P. D., Zhou, P., Stockli, D. F., & Blusztajn, J. (2019). Regional Pliocene exhumation of the Lesser Himalaya in the Indus drainage. *Solid Earth*, *10*, 647–661. https://doi.org/10.5194/se-10-647-2019

Colleps, C. L., Stockli, D. F., McKenzie, N. R., Webb, A. G., & Horton, B. K. (2019). Neogene kinematic evolution and exhumation of the NW India Himalaya: Zircon geo-/thermochronometric insights from the fold-thrust belt and foreland basin. *Tectonics*, *38*, 2059–2086. https://doi.org/10.1029/2018TC005304

Courtillot, V., Gallet, Y., Rocchia, R., Féraud, G., Robin, E., Hofmann, C., et al. (2000). Cosmic markers, 40Ar/39Ar dating and paleomagnetism of the KT sections in the Anjar Area of the Deccan large igneous province. *Earth and Planetary Science Letters*, *182*, 137–156. https://doi.org/10.1016/s0012-821x(00)00238-7

Crawford, M. B., & Searle, M. P. (1992). Field relationships and geochemistry of pre-collisional (India-Asia) granitoid magmatism in the central Karakoram, northern Pakistan. *Tectonophysics*, *206*(1–2), 171–192. https://doi.org/10.1016/0040-1951(92)90375-g

Crowley, J. L., Waters, D. J., Searle, M. P., & Bowring, S. A. (2009). Pleistocene melting and rapid exhumation of the Nanga Parbat massif, Pakistan: Age and P–T conditions of accessory mineral growth in migmatite and leucogranite. *Earth and Planetary Science Letters*, *288*(3), 408–420. https://doi.org/10.1016/j.epsl.2009.09.044

Dailey, S. K., Clift, P. D., Kulhanek, D. K., Blusztajn, J., Routledge, C. M., Calvès, G., et al. (2019). Large-scale mass wasting on the Miocene continental margin of western India. *The Geological Society of America Bulletin*, *132*(1–2), 85–112. https://doi.org/10.1130/B35158.1

DeCelles, P. G., Gehrels, G. E., Najman, Y., Martin, A. J., Carter, A., & Garzanti, E. (2004). Detrital geochronology and geochemistry of Cretaceous-Early Miocene strata of Nepal: Implications for timing and diachroneity of initial Himalayan orogenesis. *Earth and Planetary Science Letters*, *227*(3–4), 313–330. https://doi.org/10.1016/j.epsl.2004.08.019

DeCelles, P. G., Gehrels, G. E., Quade, J., LaReau, B., & Spurlin, M. (2000). Tectonic implications of U-Pb zircon ages of the Himalayan orogenic belt in Nepal. *Science*, *288*(5465), 497–499. https://doi.org/10.1126/science.288.5465.497

Deniel, C., Vidal, P., Fernandez, A., Fort, P., & Peucat, J.-J. (1987). Isotopic study of the Manaslu granite (Himalaya, Nepal): Inferences on the age and source of Himalayan leucogranites. *Contributions to Mineralogy and Petrology*, *96*(1), 78–92. https://doi.org/10.1007/bf00375529

Deptuck, M. E., Piper, D. J., Savoye, B., & Gervais, A. (2008). Dimensions and architecture of late Pleistocene submarine lobes off the northern margin of East Corsica. *Sedimentology*, *55*(4), 869–898. https://doi.org/10.1111/j.1365-3091.2007.00926.x

Dettman, D. L., Kohn, M. J., Quade, J., Ryerson, F. J., Ojha, T. P., & Hamidullah, S. (2001). Seasonal stable isotope evidence for a strong Asian monsoon throughout the past 10.7 m.y. *Geology*, *29*(1), 31–34. https://doi.org/10.1130/0091-7613(2001)029<0031:ssiefa>2.0.co;2

Donelick, R. A., O'Sullivan, P. B., & Ketcham, R. A. (2005). Apatite fission-track analysis. *Reviews in Mineralogy and Geochemistry*, *58*(1), 49–94. https://doi.org/10.1515/9781501509575-005

Dunlap, W. J., & Wysoczanski, R. (2002). Thermal evidence for Early Cretaceous metamorphism in the Shyok suture zone and age of the Khardung volcanic rocks, Ladakh, India. *Journal of Asian Earth Sciences*, *20*(5), 481–490. https://doi.org/10.1016/s1367-9120(01)00042-6

Dunlea, A. G., Murray, R. W., Sauvage, J., Spivack, A. J., Harris, R. N., & D'Hondt, S. (2015). Dust, volcanic ash, and the evolution of the South Pacific Gyre through the Cenozoic. *Paleoceanography*, *30*(8), 1078–1099. https://doi.org/10.1002/2015PA002829

Feakins, S. J., Liddy, H. M., Tauxe, L., Galy, V., Feng, X., Tierney, J. E., et al. (2020). Miocene C_4 grassland expansion as recorded by the Indus Fan. *Paleoceanography and Paleoclimatology*, *35*(6), e2020PA003856. https://doi.org/10.1029/2020PA003856

Fedo, C. M., Nesbitt, H. W., & Young, G. M. (1995). Unraveling the effects of potassium metasomatism in sedimentary rocks and paleosols, with implications for paleoweathering conditions and provenance. *Geology*, *23*, 921–924. https://doi.org/10.1130/0091-7613(1995)023<0921:uteopm>2.3.co;2

Fleitmann, D., Burns, S. J., Mudelsee, M., Neff, U., Kramers, J., Mangini, A., et al. (2003). Holocene forcing of the Indian monsoon recorded in a stalagmite from southern Oman. *Science*, *300*(5626), 1737–1739. https://doi.org/10.1126/science.1083130

Folk, R. L. (1974). *Petrology of sedimentary rocks* (p. 182). Hemphill Press.

Fraser, J. E., Searle, M. P., Parrish, R. R., & Noble, S. R. (2001). Chronology of deformation, metamorphism, and magmatism in the southern Karakoram Mountains. *The Geological Society of America Bulletin*, *113*(11), 1443–1455. https://doi.org/10.1130/0016-7606(2001)113<1443:codmam>2.0.co;2

Gaedicke, C., Schlueter, H.-U., Roeser, H.-A., Prexl, A., Schreckenberger, B., Meyer, H., et al. (2002). Origin of the northern Indus Fan and Murray Ridge, northern Arabian Sea; interpretation from seismic and magnetic imaging. *Tectonophysics*, *355*, 127–143. https://doi.org/10.1016/s0040-1951(02)00137-3

Garzanti, E., Andò, S., & Vezzoli, G. (2009). Grain-size dependence of sediment composition and environmental bias in provenance studies. *Earth and Planetary Science Letters*, *277*(3–4), 422–432. https://doi.org/10.1016/j.epsl.2008.11.007

Garzanti, E., Andò, S., & Vezzoli, G. (2020). Provenance of Cenozoic Indus Fan Sediments (IODP Sites U1456 and U1457). *Journal of Sedimentary Research*, *90*(9), 1114–1127. https://doi.org/10.2110/jsr.2019-195

Garzanti, E., Baud, A., & Mascle, G. (1987). Sedimentary record of the northward flight of India and its collision with Eurasia (Ladakh Himalaya, India). *Geodinamica Acta*, *1*(4/5), 297–312. https://doi.org/10.1080/09853111.1987.11105147

Garzanti, E., Liang, W., Andò, S., Clift, P. D., Resentini, A., Vermeesch, P., et al. (2020). Provenance of Thal Desert sand: Focused erosion in the western Himalayan syntaxis and foreland-basin deposition driven by latest Quaternary climate change. *Earth-Science Reviews*, *207*, 103220. https://doi.org/10.1016/j.earscirev.2020.103220

Garzanti, E., Vezzoli, G., Ando, S., France-Lanord, C., Singh, S. K., & Foster, G. (2004). Sand petrology and focused erosion in collision orogens: The Brahmaputra case. *Earth and Planetary Science Letters*, *220*(1–2), 157–174. https://doi.org/10.1016/s0012-821x(04)00035-4

Garzanti, E., Vezzoli, G., Ando, S., Paparella, P., & Clift, P. D. (2005). Petrology of Indus River sands: A key to interpret erosion history of the western Himalayan syntaxis. *Earth and Planetary Science Letters*, *229*(3–4), 287–302. https://doi.org/10.1016/j.epsl.2004.11.008

Gehrels, G. (2012). Detrital zircon U-Pb geochronology: Current methods and new opportunities. In C. Busby & A. Azor (Eds.), *Tectonics of sedimentary basins* (pp. 47–62). Wiley. https://doi.org/10.1002/9781444347166.ch2

Gehrels, G. E., Kapp, P., DeCelles, P., Pullen, A., Blakely, R., Weislgel, A., et al. (2011). Detrital zircon geochronology of pre-Tertiary strata in the Tibetan-Himalayan orogen. *Tectonics*, *30*(TC5016). https://doi.org/10.1029/2011TC002868

Gehrels, G. E., Valencia, V., & Ruiz, J. (2008). Enhanced precision, accuracy, efficiency, and spatial resolution of U-Pb ages by laser ablation–multicollector–inductively coupled plasma–mass spectrometry. *Geochemistry, Geophysics, Geosystems*, *9*(Q03017). https://doi.org/10.1029/2007GC001805

Guidry, M. W., & Mackenzie, F. T. (2000). Apatite weathering and the Phanerozoic phosphorus cycle. *Geology*, *28*(7), 631–634. https://doi.org/10.1130/0091-7613(2000)028<0631:awatpp>2.3.co;2

Gupta, A. K., Anderson, D. M., & Overpeck, J. T. (2003). Abrupt changes in the Asian southwest monsoon during the Holocene and their links to the North Atlantic Ocean. *Nature*, *421*, 354–356. https://doi.org/10.1038/nature01340

Hart, N. R., Stockli, D. F., & Hayman, N. W. (2016). Provenance evolution during progressive rifting and hyperextension using bedrock and detrital zircon U-Pb geochronology, Mauléon Basin, western Pyrenees. *Geosphere*, *12*(4), 1166–1186. https://doi.org/10.1130/GES01273.1

Herron, M. M. (1988). Geochemical classification of terrigenous sands and shales from core or log data. *Journal of Sedimentary Petrology*, *58*, 820–829. https://doi.org/10.1306/212f8e77-2b24-11d7-8648000102c1865d

Hildebrand, P. R., Noble, S. R., Searle, M. P., Waters, D. J., & Parrish, R. R. (2001). Old origin for an active mountain range: Geology and geochronology of the eastern Hindu Kush, Pakistan. *The Geological Society of America Bulletin*, *113*(5), 625–639. https://doi.org/10.1130/0016-7606(2001)113<0625:oofaam>2.0.co;2

Hodges, K. (2003). Geochronology and thermochronology in orogenic systems. In R. Rudnick (Ed.), *The crust* (pp. 263–292). Elsevier-Science. https://doi.org/10.1016/b0-08-043751-6/03024-3

Hodges, K. V. (2000). Tectonics of the Himalaya and southern Tibet from two perspectives. *The Geological Society of America Bulletin*, *112*(3), 324–350. https://doi.org/10.1130/0016-7606(2000)112<324:tothas>2.0.co;2

Honegger, K., Dietrich, V., Frank, W., Gansser, A., Thoni, M., & Trommsdorf, V. F. (1982). Magmatism and metamorphism in the Ladakh Himalayas (The Indus-Tsangpo suture zone). *Earth and Planetary Science Letters*, *60*, 178–194. https://doi.org/10.1016/0012-821x(82)90007-3

Howell, A. L., Bentley, S. J., Xu, K., Ferrell, R. E., Muhammad, Z., & Septama, E. (2014). Fine sediment mineralogy as a tracer of latest Quaternary sediment delivery to a dynamic continental margin: Pandora Trough, Gulf of Papua, Papua New Guinea. *Marine Geology*, *357*, 108–122. https://doi.org/10.1016/j.margeo.2014.08.003

Huyghe, P., Galy, A., Mugnier, J.-L., & France-Lanord, C. (2001). Propagation of the thrust system and erosion in the Lesser Himalaya: Geochemical and sedimentological evidence. *Geology*, *29*(11), 1007–1010. https://doi.org/10.1130/0091-7613(2001)029<1007:pottsa>2.0.co;2

Inger, S., & Harris, N. (1993). Geochemical constraints on leucogranite magmatism in the Langtang Valley, Nepal Himalaya. *Journal of Petrology*, *34*(2), 345–368. https://doi.org/10.1093/petrology/34.2.345

Jackson, S. E., Pearson, N. J., Griffin, W. L., & Belousova, E. A. (2004). The application of laser ablation-inductively coupled plasma-mass spectrometry (LA-ICP-MS) to in situ U-Pb zircon geochronology. *Chemical Geology*, *211*, 47–69. https://doi.org/10.1016/j.chemgeo.2004.06.017

Jaeger, J.-J., Courtillot, V., & Tapponnier, P. (1989). Paleontological view of the ages of the Deccan Traps, the Cretaceous/Tertiary boundary, and the India-Asia collision. *Geology*, *17*(4), 316–319. https://doi.org/10.1130/0091-7613(1989)017<0316:pvotao>2.3.co;2

Jonell, T. N., Carter, A., Böning, P., Pahnke, K., & Clift, P. D. (2017). Climatic and glacial impact on erosion patterns and sediment provenance in the Himalayan rain shadow, Zanskar River, NW India. *The Geological Society of America Bulletin*, *129*(7–8), 820–836. https://doi.org/10.1130/B31573

Jonell, T. N., Li, Y., Blusztajn, J., Giosan, L., & Clift, P. D. (2018). Signal or noise? Isolating grain size effects on Nd and Sr isotope variability in Indus delta sediment provenance. *Chemical Geology*, *485*, 56–73. https://doi.org/10.1016/j.chemgeo.2018.03.036

Khan, M. A., Stern, R. J., Gribble, R. F., & Windley, B. F. (1997). Geochemical and isotopic constraints on subduction polarity, magma sources, and palaeogeography of the Kohistan intra-oceanic arc, northern Pakistan Himalaya. *Journal of the Geological Society*, *154*, 935–946. https://doi.org/10.1144/gsjgs.154.6.0935

Khim, B.-K., Horikawa, K., Asahara, Y., Kim, J.-E., & Ikehara, M. (2019). Detrital Sr-Nd isotopes, sediment provenances, and depositional processes in the Laxmi Basin of the Arabian Sea during the last 800 kyrs. *Geological Magazine*, 1–13. https://doi.org/10.1017/S0016756818000596

Kolla, V., & Coumes, F. (1987). Morphology, internal structure, seismic stratigraphy, and sedimentation of Indus Fan. *AAPG Bulletin*, *71*, 650–677. https://doi.org/10.1306/94887889-1704-11d7-8645000102c1865d

Krol, M. A., Zeitler, P. K., & Copeland, P. (1996). Episodic unroofing of the Kohistan Batholith, Pakistan: Implications from K-feldspar thermochronology. *Journal of Geophysical Research*, *101*(B12), 28149–28164. https://doi.org/10.1029/96jb01503

Kurian, S., Nath, B. N., Kumar, N. C., & Nair, K. K. C. (2013). Geochemical and isotopic signatures of surficial sediments from the western continental shelf of India: Inferring provenance, weathering, and the nature of organic matter geochemical and isotopic signatures of sediments from the Indian west coast. *Journal of Sedimentary Research*, *83*(6), 427–442. https://doi.org/10.2110/jsr.2013.36

Lavé, J., & Avouac, J. P. (2000). Active folding of fluvial terraces across the Siwaliks Hills (Himalayas of central Nepal). *Journal of Geophysical Research*, *105*, 5735–5770. https://doi.org/10.1029/1999JB900292

Lawrence, R. L., Cox, R., Mapes, R. W., & Coleman, D. S. (2011). Hydrodynamic fractionation of zircon age populations. *GSA Bulletin*, *123*(1–2), 295–305. https://doi.org/10.1130/B30151.1

Le Fort, P., Debon, F., & Sonet, J. (1983). Petrography, geochemistry and geochronology of some samples from the Karakoram Batholith (N. Pakistan). In F. A. Shams (Ed.), *Granites of the Himalayas, Karakoram and Hindu Kush* (pp. 377–387). Punjab University.

Li, Y., Clift, P. D., Böning, P., Blusztajn, J., Murray, R. W., Ireland, T., et al. (2018). Continuous signal propagation in the Indus submarine canyon since the last deglacial. *Marine Geology*, *406*, 159–176. https://doi.org/10.1016/j.margeo.2018.09.011

Li, Y., Clift, P. D., & O'Sullivan, P. (2019). Millennial and centennial variations in zircon U-Pb and apatite fission track ages in the Quaternary Indus Submarine Canyon. *Basin Research*, *31*, 155–170. https://doi.org/10.1111/bre.12313

Malusà, M. G., Resentini, A., & Garzanti, E. (2016). Hydraulic sorting and mineral fertility bias in detrital geochronology. *Gondwana Research*, *31*, 1–19. https://doi.org/10.1016/j.gr.2015.09.002

Marsh, A. D., Parker, W. G., Stockli, D. F., & Martz, J. W. (2019). Regional correlation of the Sonsela Member (Upper Triassic Chinle Formation) and detrital U-Pb zircon data from the Sonsela Sandstone bed near the Sonsela Buttes, northeastern Arizona, USA, support the presence of a distributive fluvial system. *Geosphere*, *15*(4), 1128–1139. https://doi.org/10.1130/ges02004.1

Marsh, J. H., & Stockli, D. F. (2015). Zircon U-Pb and trace element zoning characteristics in an anatectic granulite domain: Insights from LASS-ICP-MS depth profiling. *Lithos*, *239*, 170–185. https://doi.org/10.1016/j.lithos.2015.10.017

Meigs, A. J., Burbank, D. W., & Beck, R. A. (1995). Middle-late Miocene (>10 Ma) formation of the Main Boundary Thrust in the western Himalaya. *Geology*, *23*(5), 423–426. https://doi.org/10.1130/0091-7613(1995)023<0423:mlmmfo>2.3.co;2

Molnar, P. (2001). Climate change, flooding in arid environments, and erosion rates. *Geology*, *29*(12), 1071–1074. https://doi.org/10.1130/0091-7613(2001)029<1071:ccfiae>2.0.co;2

Mukhopadhyay, G., Mukhopadhyay, S., Roychowdhury, M., & Parui, P. (2010). Stratigraphic correlation between different Gondwana basins of India. *Journal of the Geological Society of India*, *76*(3), 251–266. https://doi.org/10.1007/s12594-010-0097-6

Myrow, P. M., Hughes, N. C., Derry, L. A., McKenzie, R. N., Jiang, G., Webb, A. A. G., et al. (2015). Neogene marine isotopic evolution and the erosion of Lesser Himalayan strata: Implications for Cenozoic tectonic history. *Earth and Planetary Science Letters*, *417*, 142–150. https://doi.org/10.1016/j.epsl.2015.02.016

Najman, Y. (2006). The detrital record of orogenesis: A review of approaches and techniques used in the Himalayan sedimentary basins. *Earth-Science Reviews*, *74*(1–2), 1–72.

Najman, Y., Appel, E., Boudagher-Fadel, M., Bown, P., Carter, A., Garzanti, E., et al. (2010). Timing of India-Asia collision: Geological, biostratigraphic, and palaeomagnetic constraints. *Journal of Geophysical Research*, *115*(B12416). https://doi.org/10.1029/2010JB007673

Najman, Y., Bickle, M., Garzanti, E., Pringle, M., Barfod, D., Brozovic, N., et al. (2009). Reconstructing the exhumation history of the Lesser Himalaya, NW India, from a multitechnique provenance study of the foreland basin Siwalik Group. *Tectonics*, *28*(TC5018). https://doi.org/10.1029/2009TC002506

Nesbitt, H. W., Markovics, G., & Price, R. C. (1980). Chemical processes affecting alkalis and alkaline earths during continental weathering. *Geochimica et Cosmochimica Acta*, *44*, 1659–1666. https://doi.org/10.1016/0016-7037(80)90218-5

Pandey, D. K., Clift, P. D., Kulhanek, D. K., Andò, S., Bendle, J. A. P., Bratenkov, S., et al. (2016a). Site U1456. In D. K. Pandey, P. D. Clift, & D. K. Kulhanek (Eds.), *Arabian Sea Monsoon. Proceedings of the International Ocean Discovery Program*. International Ocean Discovery Program. https://doi.org/10.14379/iodp.proc.355.103.2016

Pandey, D. K., Clift, P. D., Kulhanek, D. K., Andò, S., Bendle, J. A. P., Bratenkov, S., et al. (2016b). Site U1457. In D. K. Pandey, P. D. Clift, & D. K. Kulhanek (Eds.), *Arabian Sea Monsoon. Proceedings of the International Ocean Discovery Program*. International Ocean Discovery Program. https://doi.org/10.14379/iodp.proc.355.104.2016

Pandey, D. K., Clift, P. D., Kulhanek, D. K., & Expedition 355 Scientists. (2016c). Arabian Sea monsoon. *Proceedings of the International Ocean Discovery Program*, *355*. https://doi.org/10.14379/iodp.proc.355.2016

Pandey, D. K., Clift, P. D., Kulhanek, D. K., & Expedition 355 Scientists. (2016d). Arabian Sea Monsoon: Expedition summary. *Proceedings of the International Ocean Discovery Program*, *355*, 1–32. https://doi.org/10.14379/iodp.proc.355.101.2016

Pandey, O. P., Agrawal, P. K., & Negi, J. G. (1995). Lithospheric structure beneath Laxmi Ridge and late Cretaceous geodynamic events. *Geo-Marine Letters*, *15*, 85–91. https://doi.org/10.1007/bf01275411

Parrish, R. R., & Hodges, K. V. (1996). Isotopic constraints on the age and provenance of the Lesser and Greater Himalayan sequences, Nepalese Himalaya. *The Geological Society of America Bulletin*, *108*(7), 904–911. https://doi.org/10.1130/0016-7606(1996)108<0904:icotaa>2.3.co;2

Parrish, R. R., & Tirrul, R. (1989). U-Pb age of the Baltoro granite, Northwest Himalaya, and implications for monazite U-Pb systematics. *Geology*, *17*, 1076–1079. https://doi.org/10.1130/0091-7613(1989)017<1076:upaotb>2.3.co;2

Paton, C., Hellstrom, J., Paul, B., Woodhead, J., & Hergt, J. (2011). Iolite: Freeware for the visualisation and processing of mass spectrometric data. *Journal of Analytical Atomic Spectrometry*, *26*(12), 2508–2518. https://doi.org/10.1039/c1ja10172b

Petrus, J. A., & Kamber, B. S. (2012). VizualAge: A novel approach to laser ablation ICP-MS U-Pb geochronology data reduction. *Geostandards and Geoanalytical Research*, *36*(3), 247–270. https://doi.org/10.1111/j.1751-908x.2012.00158.x

Quade, J., Cerling, T. E., & Bowman, J. R. (1989). Development of Asian monsoon revealed by marked ecological shift during the latest Miocene in northern Pakistan. *Nature*, *342*(6246), 163–166. https://doi.org/10.1038/342163a0

Radhakrishna, T., Bansal, B. K., & Ramakrishna, C. (2021). Geodynamic events leading to formation of passive western continental margin of India. *Journal of Geodynamics*, *148*, 101878. https://doi.org/10.1016/j.jog.2021.101878

Ravikant, V., Wu, F. Y., & Ji, W. Q. (2009). Zircon U-Pb and Hf isotopic constraints on petrogenesis of the Cretaceous-Tertiary granites in eastern Karakoram and Ladakh, India. *Lithos*, *110*, 153–166. https://doi.org/10.1016/j.lithos.2008.12.013

Robinson, D. M., DeCelles, P. G., & Copeland, P. (2006). Tectonic evolution of the Himalayan thrust belt in western Nepal; implications for channel flow models. *The Geological Society of America Bulletin*, *118*(7–8), 865–885. https://doi.org/10.1130/b25911.1

Roddaz, M., Said, A., Guillot, S. P., Antoine, P. O., Montel, J. M., Martin, F., et al. (2011). Provenance of Cenozoic sedimentary rocks from the Sulaiman fold and thrust belt, Pakistan: Implications for the palaeogeography of the Indus drainage system. *Journal of the Geological Society*, *168*, 499–516. https://doi.org/10.1144/0016-76492010-100

Rolland, Y., Mahéo, G., Guillot, S., & Pecher, A. (2001). Tectono-metamorphic evolution of the Karakorum Metamorphic complex (Dassu–Askole area, NE Pakistan): Exhumation of mid-crustal HT–MP gneisses in a convergent context. *Journal of Metamorphic Geology*, *19*(6), 717–737. https://doi.org/10.1046/j.0263-4929.2001.00342.x

Rolland, Y., Picard, C., Pecher, A., Lapierre, H., Bosch, D., & Keller, F. (2002). The Cretaceous Ladakh arc of NW Himalaya—Slab melting and melt–mantle interaction during fast northward drift of Indian Plate. *Chemical Geology*, *182*, 139–178. https://doi.org/10.1016/s0009-2541(01)00286-8

Routledge, C. M., Kulhanek, D. K., Tauxe, L., Scardia, G., Singh, A. D., Steinke, S., et al. (2020). Revised geological timescale for IODP Sites U1456 and U1457. *Geological Magazine*, *157*(6), 961–978. https://doi.org/10.1017/S0016756819000104

Schärer, U., Copeland, P., Harrison, T. M., & Searle, M. P. (1990). Age, cooling history, and origin of post-collisional leucogranites in the Karakoram Batholith; a multi-system isotope study. *The Journal of Geology*, *98*(2), 233–251.

Schärer, U., Xu, R.-H., & Allègre, C. J. (1984). U-Pb geochronology of Gangdese (Transhimalaya) plutonism in the Lhasa-Xigaze region, Tibet. *Earth and Planetary Science Letters*, *69*(2), 311–320.

Searle, M. P. (1996). Cooling history, erosion, exhumation and kinematics of the Himalaya-Karakoram-Tibet orogenic belt. In A. Yin & T. M. Harrison (Eds.), *The tectonic evolution of Asia* (pp. 110–137). Cambridge University Press.

Searle, M. P., & Phillips, R. J. (2007). Relationships between right-lateral shear along the Karakoram Fault and metamorphism, magmatism, exhumation and uplift; evidence from the K2-Gasherbrum-Pangong ranges, north Pakistan and Ladakh. *Journal of the Geological Society*, *164*(2), 439–450. https://doi.org/10.1144/0016-76492006-072

Searle, M. P., Rex, A. J., Tirrul, R., Rex, D. C., Barnicoat, A., & Windley, B. F. (1989). Metamorphic, magmatic and tectonic evolution of the Central Karakoram in the Biafo-Baltoro-Hushe regions of north Pakistan. *Geological Society of America Special Paper*, *232*, 47–73. https://doi.org/10.1130/spe232-p47

Shanmugam, G., & Moiola, R. (1991). Types of submarine fan lobes: Models and implications. *AAPG Bulletin*, *75*(1), 156–179. https://doi.org/10.1306/0c9b276d-1710-11d7-8645000102c1865d

Shuaib, S. M. (1982). Geology and hydrocarbon potential of offshore Indus Basin, Pakistan. *AAPG Bulletin*, *66*, 940–946. https://doi.org/10.1306/03b5a363-16d1-11d7-8645000102c1865d

Singh, S., Kumar, R., Barley, M. E., & Jain, A. K. (2007). SHRIMP U-Pb ages and depth of emplacement of Ladakh batholith, eastern Ladakh, India. *Journal of Asian Earth Sciences*, *30*(3), 490–503. https://doi.org/10.1016/j.jseaes.2006.12.003

Singh, S., Parkash, B., Awasthi, A. K., & Kumar, S. (2011). Late Miocene record of palaeovegetation from Siwalik palaeosols of the Ramnagar sub-basin, India. *Current Science*, *100*(2), 213–222.

Singh, S. K., & France-Lanord, C. (2002). Tracing the distribution of erosion in the Brahmaputra watershed from isotopic compositions of stream sediments. *Earth and Planetary Science Letters*, *202*(3–4), 645–662. https://doi.org/10.1016/s0012-821x(02)00822-1

Spencer, C. J., Kirkland, C. L., & Taylor, R. J. M. (2016). Strategies towards statistically robust interpretations of in situ U-Pb zircon geochronology. *Geoscience Frontiers*, *7*(4), 581–589. https://doi.org/10.1016/j.gsf.2015.11.006

Stephenson, B. J., Searle, M. P., Waters, D. J., & Rex, D. C. (2001). Structure of the main central thrust zone and extrusion of the High Himalayan deep crustal wedge, Kishtwar-Zanskar Himalaya. *Journal of the Geological Society*, *158*(4), 637–652. https://doi.org/10.1144/jgs.158.4.637

Stewart, R. J., Hallet, B., Zeitler, P. K., Malloy, M. A., Allen, C. M., & Trippett, D. (2008). Brahmaputra sediment flux dominated by highly localized rapid erosion from the easternmost Himalaya. *Geology*, *36*(9), 711–714. https://doi.org/10.1130/G24890A.1

Sundell, K., & Saylor, J. E. (2017). Unmixing detrital geochronology age distributions. *Geochemistry, Geophysics, Geosystems*, *18*, 2872–2886. https://doi.org/10.1002/2016gc006774

Suzuki, K., Yamamoto, M., & Seki, O. (2020). Late Miocene changes in C_3, C_4 and aquatic plant vegetation in the Indus River basin: Evidence from leaf wax $\delta^{13}C$ from Indus Fan sediments. *Geological Magazine*, *157157*(6156), 979–988. https://doi.org/10.1017/S0016756819001109

Taylor, S. R., & McLennan, S. M. (1995). The geochemical evolution of the continental crust. *Reviews of Geophysics*, *33*, 241–265. https://doi.org/10.1029/95rg00262

Thiede, R. C., Bookhagen, B., Arrowsmith, J. R., Sobel, E. R., & Strecker, M. R. (2004). Climatic control on rapid exhumation along the Southern Himalayan Front. *Earth and Planetary Science Letters*, *222*(3–4), 791–806. https://doi.org/10.1016/j.epsl.2004.03.015

Thiede, R. C., Ehlers, T. A., Bookhagen, B., & Strecker, M. R. (2009). Erosional variability along the northwest Himalaya. *Journal of Geophysical Research*, *114*, F01015. https://doi.org/10.1029/2008JF001010

Tromans, D. (2006). Solubility of crystalline and metamict zircon: A thermodynamic analysis. *Journal of Nuclear Materials*, *357*(1), 221–233. https://doi.org/10.1016/j.jnucmat.2006.06.012

Vermeesch, P. (2004). How many grains are needed for a provenance study? *Earth and Planetary Science Letters*, *224*, 351–441. https://doi.org/10.1016/j.epsl.2004.05.037

Vermeesch, P., Resentini, A., & Garzanti, E. (2016). An R package for statistical provenance analysis. *Sedimentary Geology*, *336*, 14–25. https://doi.org/10.1016/j.sedgeo.2016.01.009

Vögeli, N., Najman, Y., van der Beek, P., Huyghe, P., Wynn, P. M., Govin, G., et al. (2017). Lateral variations in vegetation in the Himalaya since the Miocene and implications for climate evolution. *Earth and Planetary Science Letters*, *471*, 1–9. https://doi.org/10.1016/j.epsl.2017.04.037

Wallis, D., Carter, A., Phillips, R. J., Parsons, A. J., & Searle, M. P. (2016). Spatial variation in exhumation rates across Ladakh and the Karakoram: New apatite fission track data from the Eastern Karakoram, NW India. *Tectonics*, *35*, 704–721. https://doi.org/10.1002/2015TC003943

Wallis, D., Phillips, R. J., & Lloyd, G. E. (2014). Evolution of the Eastern Karakoram Metamorphic Complex, Ladakh, NW India, and its relationship to magmatism and regional tectonics. *Tectonophysics*, *626*, 41–52. https://doi.org/10.1016/j.tecto.2014.03.023

Webb, A. A. G. (2013). Preliminary palinspastic reconstruction of Cenozoic deformation across the Himachal Himalaya (northwestern India). *Geosphere*, *9*, 572–587. https://doi.org/10.1130/GES00787.1

Weinberg, R. F., & Dunlap, W. J. (2000). Growth and deformation of the Ladakh Batholith, Northwest Himalayas: Implications for timing of continental collision and origin of calcalkaline batholiths. *The Journal of Geology*, *108*, 303–320. https://doi.org/10.1086/314405

Whipple, K. X. (2009). The influence of climate on the tectonic evolution of mountain belts. *Nature Geoscience*, *2*, 1–8. https://doi.org/10.1038/ngeo413

White, A. F., & Brantley, S. L. (1995). *Chemical weathering rates of silicate minerals* (p. 581). Mineralogical Society of America. https://doi.org/10.1515/9781501509650-fm

White, N. M., Pringle, M., Garzanti, E., Bickle, M., Najman, Y., Chapman, H., et al. (2002). Constraints on the exhumation and erosion of the High Himalayan Slab, NW India, from foreland basin deposits. *Earth and Planetary Science Letters*, *195*, 29–44. https://doi.org/10.1016/s0012-821x(01)00565-9

Whittington, A., Foster, G., Harris, N., Vance, D., & Ayres, M. (1999). Lithostratigraphic correlations in the western Himalaya – An isotopic approach. *Geology*, *27*(7), 585–588. https://doi.org/10.1130/0091-7613(1999)027<0585:lcitwh>2.3.co;2

Wilson, S. A. (1997). Data compilation for USGS reference material BHVO-2, Hawaiian Basalt. *US Geological Survey Open-File Report*, 2–3.

Wobus, C. W., Hodges, K. V., & Whipple, K. X. (2003). Has focused denudation sustained active thrusting at the Himalayan topographic front? *Geology*, *31*(10), 861–864. https://doi.org/10.1130/g19730.1

Yang, S., Zhang, F., & Wang, Z. (2012). Grain size distribution and age population of detrital zircons from the Changjiang (Yangtze) River system, China. *Chemical Geology*, *296–297*, 26–38. https://doi.org/10.1016/j.chemgeo.2011.12.016

Yin, A., Dubey, C. S., Kelty, T. K., Webb, A. A. G., Harrison, T. M., Chou, C. Y., et al. (2010). Geologic correlation of the Himalayan orogen and Indian craton: Part 2. Structural geology, geochronology, and tectonic evolution of the Eastern Himalaya. *GSA Bulletin*, *122*(3–4), 360–395. https://doi.org/10.1130/B26461.1

Zeilinger, G., Burg, J. P., Schaltegger, U., & Seward, D. (2001). New U/Pb and fission track ages and their implication for the tectonic history of the lower Kohistan Arc Complex, northern Pakistan. *Journal of Asian Earth Sciences*, *19*(3S), 79–81.

Zeitler, P. K., & Chamberlain, C. P. (1991). Petrogenetic and tectonic significance of young leukogranites from the northwestern Himalaya, Pakistan. *Tectonics*, *10*(4), 729–741. https://doi.org/10.1029/91tc00168

Zeitler, P. K., Chamberlain, C. P., & Smith, H. A. (1993). Synchronous anatexis, metamorphism, and rapid denudation at Nanga-Parbat (Pakistan Himalaya). *Geology*, *21*(4), 347–350. https://doi.org/10.1130/0091-7613(1993)021<0347:samard>2.3.co;2

Zeitler, P. K., Sutter, J. F., Williams, I. S., Zartman, R. E., & Tahirkheli, R. A. K. (1989). Geochronology and temperature history of the Nanga Parbat-Haramosh Massif, Pakistan. In L. L. Malinconico & R. J. Lillie (Eds.), *Tectonics of the western Himalayas* (pp. 1–22). Geological Society of America. https://doi.org/10.1130/spe232-p1

Zhou, P., Carter, A., Li, Y., & Clift, P. D. (2019). Slowing rates of regional exhumation in the western Himalaya: Fission track evidence from the Indus Fan. *Geological Magazine*. https://doi.org/10.1017/S001675681900092X

Zhuang, G., Najman, Y., Guillot, S., Roddaz, M., Antoine, P.-O., Métaise, G., et al. (2015). Constraints on the collision and the pre-collision tectonic configuration between India and Asia from detrital geochronology, thermochronology, and geochemistry studies in the lower Indus basin, Pakistan. *Earth and Planetary Science Letters*, *432*, 363–373. https://doi.org/10.1016/j.epsl.2015.10.026

Zhuang, G., Najman, Y., Tian, Y., Carter, A., Gemignani, L., Wijbrans, J., et al. (2018). Insights into the evolution of the Hindu Kush-Kohistan-Karakoram from modern river sand detrital geo- and thermochronological studies. *Journal of the Geological Society*. https://doi.org/10.1144/jgs2018-007